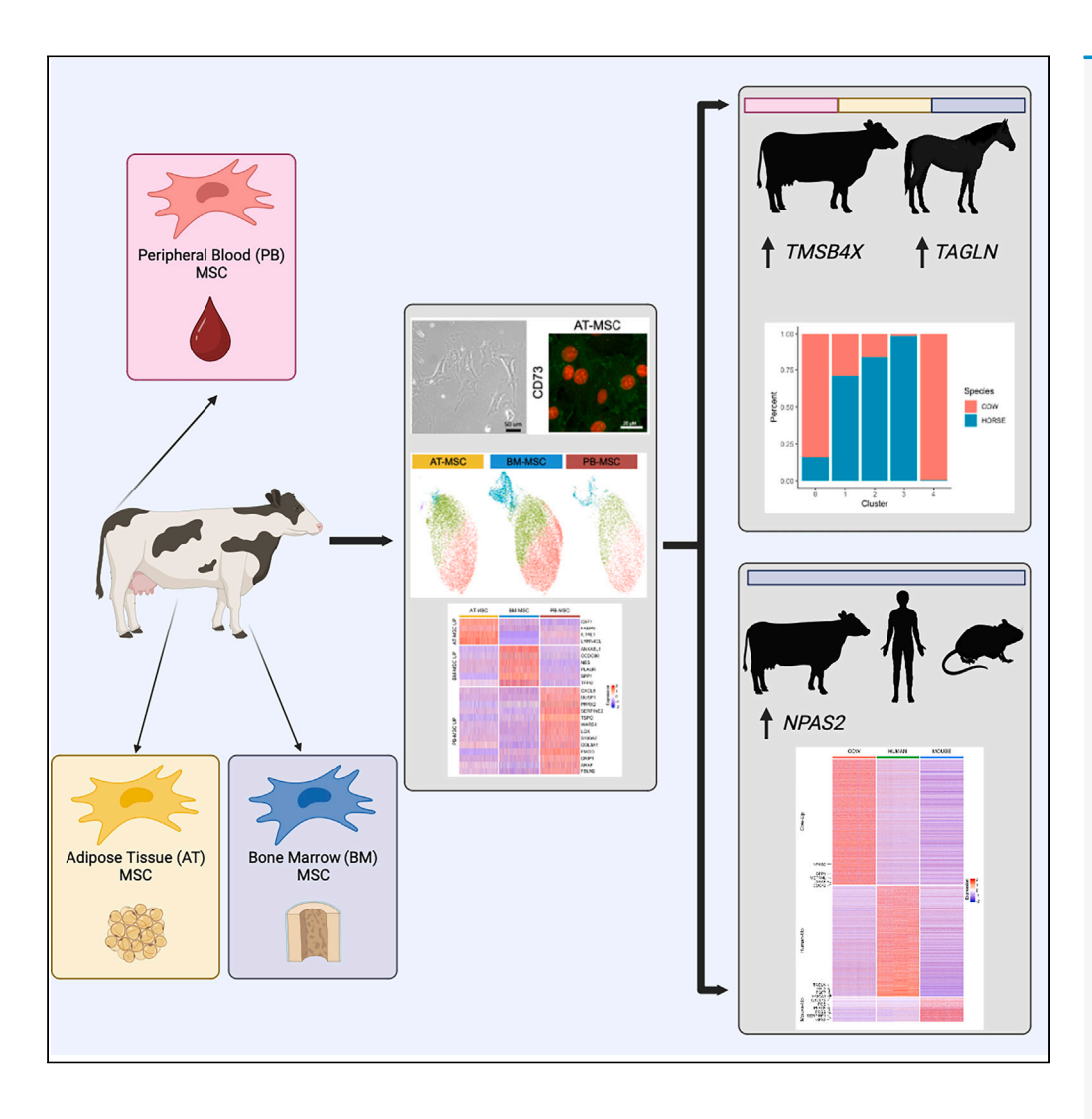
iScience



Article

Comparative transcriptomic analysis of bovine mesenchymal stromal cells reveals tissue-source and species-specific differences



Nikola Danev, Guangsheng Li, Jingyue (Ellie) Duan, Gerlinde R. Van de Walle

jd774@cornell.edu (J.D.) grv23@cornell.edu (G.R.V.d.W.)

Highlights

Bovine MSCs can be isolated from adipose, bone marrow, and blood

MSC transcriptomes vary by tissue source and species of origin

Human BM-MSCs share more transcripts with cows than with mice

Bovine BM-MSCs present a viable model for translational studies

Danev et al., iScience 27, 108886 February 16, 2024 © 2024 The Author(s). https://doi.org/10.1016/ j.isci.2024.108886



iScience



Article

Comparative transcriptomic analysis of bovine mesenchymal stromal cells reveals tissue-source and species-specific differences

Nikola Danev,^{1,3} Guangsheng Li,^{2,3} Jingyue (Ellie) Duan,^{2,*} and Gerlinde R. Van de Walle^{1,4,*}

SUMMARY

Mesenchymal stromal cells (MSCs) have the potential to be used as therapeutics, but their efficacy varies due to cellular heterogeneity, which is not fully understood. After characterizing donor-matched bovine MSC from adipose tissue (AT), bone marrow (BM), and peripheral blood (PB), we performed single-cell RNA sequencing (scRNA-seq) to evaluate overarching similarities and differences across these three tissue-derived MSCs. Next, the transcriptomic profiles of the bovine MSCs were compared to those of equine MSCs, derived from the same tissue sources and previously published by our group, and revealed species-specific differences. Finally, the transcriptomic profile from bovine BM-MSCs was compared to mouse and human BM-MSCs and demonstrated that bovine BM-MSCs share more common functionally relevant gene expression profiles with human BM-MSCs than compared to murine BM-MSCs. Collectively, this study presents the cow as a potential non-traditional animal model for translational MSC studies based on transcriptomic profiles similar to human MSCs.

INTRODUCTION

Mesenchymal stromal cells (MSCs) are a multipotent cell population, isolated from adult stroma, that has been shown to have regenerative and immunomodulatory properties, making them a valuable source of potential therapeutics across multiple species. ¹⁻⁶ However, despite an increasing number of studies and trials evaluating the therapeutic potential of MSCs, their use in clinical settings has remained low. ^{7,8} Notably, in the United States, the Food and Drug Administration has not granted approval to any MSC treatments in human medicine. This is in part due to the substantial variability between MSC cultures, ^{9,10} and the lack of standardized MSC characteristics across different tissue sources. ¹¹

MSCs have been isolated successfully from numerous species, including but not limited to humans, mice, cows, rats, cats, horses, and chickens. ^{1,3,10,12–16} MSCs are commonly isolated from adipose tissue (AT), bone marrow (BM), peripheral blood (PB), umbilical cord, placenta, dental pulp, and other adult stromal tissues. ^{10,17} Guidelines have been proposed for the uniform identification and classification of human MSCs, which include the ability of the cells to (1) adhere directly to plastic, (2) differentiate into adipo-, chondro-, and osteocytes, and (3) stain either positive or negative for a predefined panel of surface markers using flow cytometry. ¹⁸ However, recent findings have identified variability in the expression of known markers in human MSCs based on tissue of origin ^{11,19} and MSCs from veterinary species have shown inconsistent and species-specific expression patterns of these markers. ^{3,10,20}

Previous work has compared MSC populations across tissue of origin, with most of these comparisons being done with human and mouse MSCs and yielding variable findings. ²¹ For example, one group reported that human BM- and AT-MSCs share similar effects on the inhibition of T cell proliferation, ²² while others found that either AT-MSCs or BM-MSCs were more potent T cell inhibitors than the other, depending on the study. ^{23,24} The variability in these findings may, in part, be attributable to donor-specific differences. For example, a difference in osteogenic differentiation potential was found between different donors of both feline and canine MSCs. ²⁵ To mitigate these effects, a donor-matching experimental design has been employed for robust comparisons. Several studies with donor-matched MSCs from humans, rats, and horses have confirmed that phenotypic differences exist between tissue sources, donors, and species. ^{10,26,27}

An additional obstacle to canonical MSC research using non-traditional animal models is the lack of commercially available and cross-reactive antibodies markers used to identify human, mouse, and rat MSCs. ²⁸ For example, recent attempts to find cross-reactive antibodies for CD105 and CD106 in the bovine model have been unsuccessful. ²⁰ However, RNA sequencing can overcome this challenge by characterizing cell populations based on their expression of mRNA transcripts to identify common protein surface markers. ²⁹ Single-cell RNA sequencing (scRNA-seq) adds an additional layer of resolution unavailable in traditional immunophenotyping by allowing for the segregation and characterization of single cells into subgroups based on their mRNA profiles. ³⁰ By implementing scRNA-seq in MSC research, the heterogeneity of

^{*}Correspondence: jd774@cornell.edu (J.D.), grv23@cornell.edu (G.R.V.d.W.) https://doi.org/10.1016/j.isci.2024.108886



¹Baker Institute for Animal Health, College of Veterinary Medicine, Cornell University, Ithaca, NY 14853, USA

²Department of Animal Science, College of Agriculture and Life Sciences, Cornell University, Ithaca, NY 14853, USA

³These authors contributed equally

⁴Lead contact



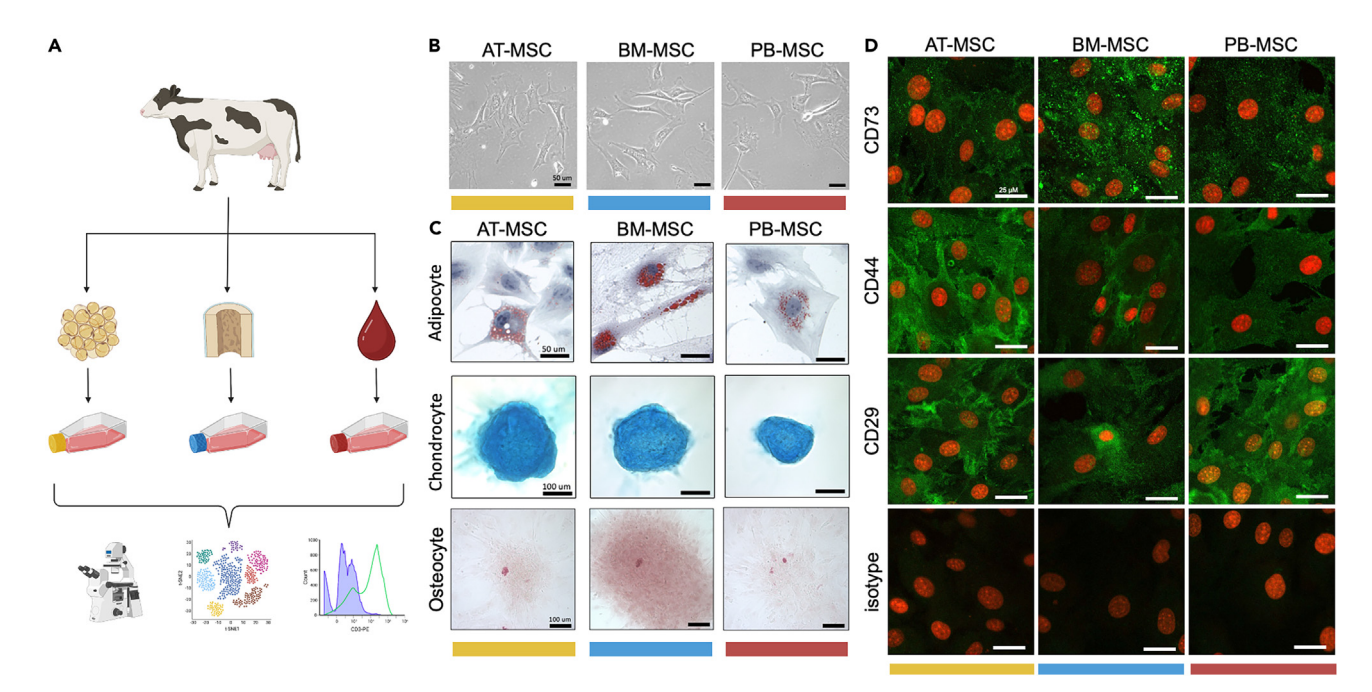


Figure 1. Experimental pipeline overview and phenotypic analysis of primary MSCs

(A) Schematic figure of the experimental pipeline. Bovine tissues were collected and MSCs isolated from adipose tissue (AT, yellow), bone marrow (BM, blue), and peripheral blood (PB, red). Each MSC was subjected to phenotypic, involving imaging for morphological characteristics, and functional analyses, i.e., in vitro differentiation assays. Moreover, each MSC source was analyzed for gene expression, using single-cell RNA sequencing (scRNA-seq) and quantitative (q)RT-PCR, and for protein expression, using flow cytometry.

- (B) Representative images of AT-, BM-, and PB-MSCs exhibiting a plastic-adherent, spindle-like morphology. Scale bar = 50 µm.
- (C) Representative images of AT-, BM-, and PB-MSCs that differentiated into adipocytes (Oil Red O), chondrocytes (Alcian blue), and osteocytes (Alizarin Red), when cultured in differentiation medium. Scale bar = $50 \mu m$ for adipocytes, $100 \mu m$ for chondrocytes and osteocytes.
- (D) Representative immunofluorescent images of AT-, BM-, and PB-MSCs exhibiting positive expression of CD73, CD44, and CD29. A negative control isotype is included; counterstaining for nuclei is in red, whereas green indicates the presence of each target protein. Scale bar = $25 \, \mu m$.

MSC populations from non-traditional animal models can be assessed at unprecedented resolutions at the tissue-specific level, as evidenced in the equine model. ¹⁰ Moreover, by eliminating the need for cross-reactive antibodies for immunophenotyping, scRNA-seq allows for more direct comparisons of cell populations across multiple species.

Despite many studies focusing on understanding MSCs from different veterinary species, few studies reported on the comparative characterization of bovine MSCs. With 80% of the global population regularly consuming dairy products³¹ and an expected continuous increase in the number of cows,³² it is important to gain a better understanding of bovine MSCs. These cells have the potential to enhance therapeutic approaches and serve as a valuable animal model for translational studies in human regenerative medicine research.

In this study, we isolated and characterized donor-matched AT-, BM-, and PB-MSCs from cows using canonical methods such as tri-lineage differentiation assays and flow cytometry-based immunophenotyping. We also assessed their transcriptomic heterogeneity using scRNA-seq and validated our findings using reverse transcription quantitative PCR. Moreover, we used pre-existing datasets to compare our findings in bovine MSCs to those of another veterinary species, the horse, as well as human and murine MSCs.

RESULTS

Donor-matched primary bovine MSCs present uniform morphology and readily differentiate across tissue sources

Donor-matched bovine MSCs were isolated from AT, BM, and PB, from a single donor and characterized using microscopy, scRNA-seq, and flow cytometry (Figure 1A). Phase-contrast microscopy was used to reveal plastic-adherent cells with a spindle-like morphology (Figure 1B), which is consistent with bovine MSCs characterized by other groups, ^{20,33,34} as well as MSCs from other species. ^{3,10,27,35} Moreover, bovine MSCs were able to differentiate into adipocytes, chondrocytes, and osteocytes (Figure 1C), again, consistent with both human MSCs, ¹⁸ as well as MSCs from other species. ^{20,29} Of note, however, is that the bovine BM-MSCs differentiated more readily into osteocytes when compared to AT- and PB-MSCs. This is similar to human BM-MSCs, which were found to have the greatest osteogenic differentiation potential when compared to MSCs derived from multiple other tissue sources, including AT-MSCs. ³⁶ Moreover, human BM-MSCs showed remarkable similarity to MSC-derived osteocytes at the transcriptomic level. ³⁶ Lastly, MSCs were characterized by immunofluorescent imaging using three positive MSC markers (CD73, CD44, and CD29), and cells from all three tissue sources were found to express these three markers (Figure 1D).



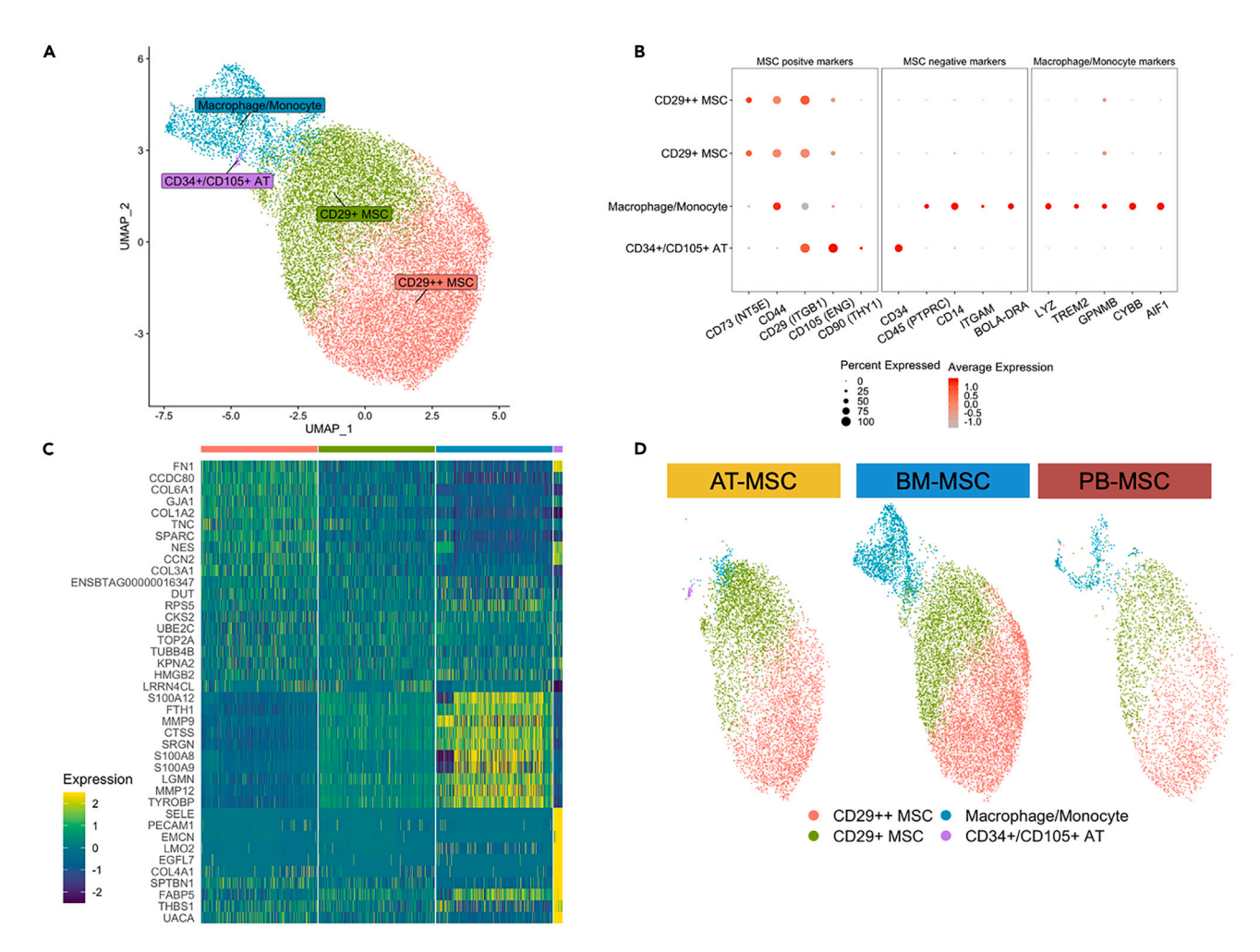


Figure 2. scRNA-seq reveals four distinct clusters across three tissue sources

(A) A UMAP projection of all MSCs combined from three tissue sources and annotated into four distinct clusters of cells.

(B) Dot plot indicating the annotation of four clusters using the relative expression of known positive and negative marker genes for MSCs, as well as markers for macrophages/monocytes.

(C) Heatmap depicting the expression of the top 10 differentially expressed markers in four clusters (D) UMAP showing the prevalence of cells belonging to four clusters in each of the three tissue sources separately. CD34+/CD105+ AT is only found in the AT-MSCs. See also Figure S1.

scRNA-seq reveals tissue source-independent gene expression profiles for the majority of cells within MSC populations

scRNA-seq was utilized to identify cell types within bovine MSC cultures from the three tissue sources and assess their level of tissue of origin heterogeneity. Overall, BM-MSCs represented about 53% (10,497 cells) of the total cells (19,694 cells) with AT-MSCs constituting about 31% (6,121 cells) and PB-MSCs about 16% (3,076 cells) (Figure S1A). All three cell types had similar numbers of unique molecular identifiers per cell, as well as genes per cell (Figure S1B).

When visualizing the combined transcriptomic data of all three tissue sources, four clusters were identified across the three MSC groups, with the two major clusters representing MSCs (CD29⁺ and CD29⁺⁺ MSC), followed by a cluster of macrophages-like cells (macrophage/monocyte), and finally, a small distinct cluster consisting exclusively of AT-MSC cells (CD34⁺/CD105⁺ AT) (Figure 2A). To annotate these clusters, known markers for the identification of MSCs from veterinary species, ¹⁰ together with markers for immune cells in cows, ^{37,38} were used. Two MSC clusters strongly expressed NT5E (CD73), CD44 (CD44), ITGB1 (CD29), and ENG (CD105), all known markers of MSCs in veterinary species. However, the expression of ITGB1 (CD29) differed, with one MSC cluster expressing more than the other, therefore being annotated as CD29⁺ and CD29⁺⁺ MSC (Figure 2B). The third largest cluster, macrophage/monocyte, expressed markers characteristic of these cell types, such as LYZ, TREM2, GPNMB, CYBB, and AIF1 (Figure 2B). Lastly, the small distinct cluster of AT-MSCs only expressed ENG (CD105), ITGB1 (CD29), and THY1 (CD90) from the MSC-positive marker subset. Additionally, it expressed CD34 (CD34), a known negative marker for MSCs, and thus was named cluster CD34⁺/CD105⁺ AT (Figure 2B). Cell distribution by clusters is summarized as absolute numbers by tissue source (Figure S1C) and as percentages of tissue source in each cluster (Figure S1D).



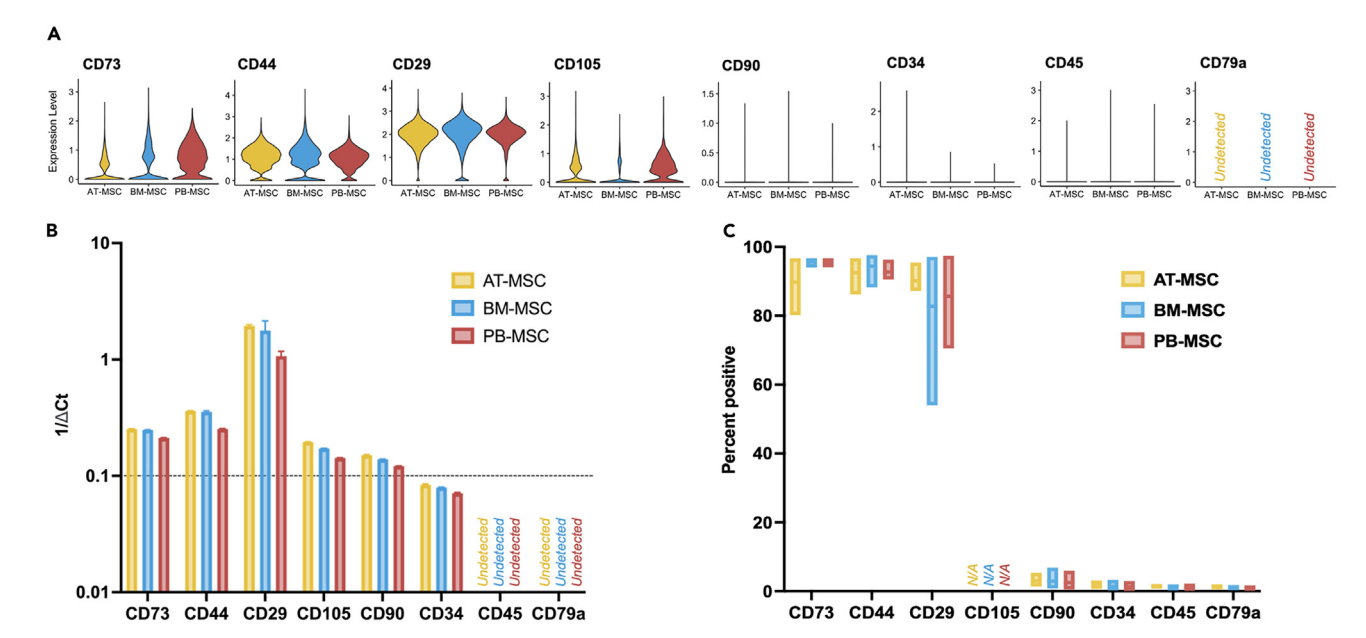


Figure 3. MSC marker expression is similar at the transcriptomic and proteomic levels

(A) Violin plots were generated from scRNA-seq data for each of the following positive and negative MSC markers: CD73, CD44, CD29, CD105, CD90, CD34, CD45, CD79a.

(B) Bar chart on a logarithmic axis of scRNA-seq marker expression findings using qPCR. Data shown as $1/\Delta Ct$; Ct counts normalized to GAPDH. N = 3. Error bars = standard deviation.

(C) Boxplot of flow cytometry data for protein expression levels of surface markers considered in transcriptomic analyses. CD105 was not shown due to lack of species cross-reactivity. N = 3. Yellow indicates AT-MSCs, blue indicates BM-MSCs, and red indicates PB-MSCs. See also Table S5.

A heatmap representing the top 10 most differentially expressed genes in each cluster within the combined MSC dataset found overall similar gene expression patterns between cluster CD29⁺⁺ MSC and CD29⁺ MSC, while the enrichment of top genes in macrophage/monocyte and CD34+/CD105+ AT clusters was more distinct (Figure 2C). Specifically, the macrophage/monocyte cluster was found to enrich more genes coding for the S100A protein family and the matrix metalloprotease protein family compared to the other clusters. Finally, the small CD34+/CD105+ AT cluster strongly expressed a variety of genes, including SELE, PECAM1, EMCN, LMO2, and others, which were all lowly expressed in the other clusters (Figure 2C).

When separating the single-cell data by tissue of origins into distinct UMAPs, it was confirmed that the three largest clusters (i.e., CD29⁺ MSC, CD29⁺⁺ MSC, and macrophage/monocyte) were found in MSC cultures from all three tissues, whereas cluster CD34⁺/CD105⁺ AT was only present in the AT-derived MSC (Figure 2D). Additionally, AT-MSCs had the lowest abundance of immune cells out of all three tissue groups (Figure 2D).

MSC marker gene and protein expression patterns are consistent between bovine MSCs from different tissue sources

The expression patterns of known MSC marker genes were compared across AT, BM, and PB using the scRNA-seq data and verified using quantitative PCR (qPCR). As expected, CD73, CD44, CD29, and CD105 were found to be strongly expressed in all three tissue sources, confirming the mesenchymal and pluripotent identities of these cells (Figure 3A). However, expression of CD90, a positive marker for human and equine MSCs, ^{10,18} was notably low (Figure 3A). Markers expected to be negative in human MSCs, such as CD34, CD45, and CD79a, were also found to be either lowly or not at all expressed (Figure 3A). These results were confirmed by qPCR, where the relative expression of each target gene was compared to that of the standard housekeeping gene, *GAPDH* (Figure 2B).

To validate the transcriptomic findings at the protein level, flow cytometry was used to evaluate protein expression. The protein markers CD73, CD44, and CD29 were found to be highly expressed, and CD90, CD34, CD45, and CD79a expression was found in <5% of MSCs (Figure 3C). We were unable to verify protein expression of CD105 due to a lack of available cross-reactive antibodies.²⁰

Pairwise comparison of bovine MSCs reveals tissue of origin-specific enrichment and depletion of select transcriptomic markers and signaling pathways

To gain a global understanding of how gene expression varies in bovine MSCs derived from different tissues, pairwise differential expression analysis was performed in MSCs using the model-based analysis of single-cell transcriptomics, ³⁹ with a random effect for sequencing depth. Using this approach, 625, 724, and 552 differentially expressed genes (DEGs) were found when comparing AT- with BM-MSCs, AT- with PB-MSCs, and BM- with PB-MSCs, respectively (adjusted p value (padj) < 0.05, log2 fold change > 0.3) (Figure 4A; Table S1). To identify associated

iScience Article



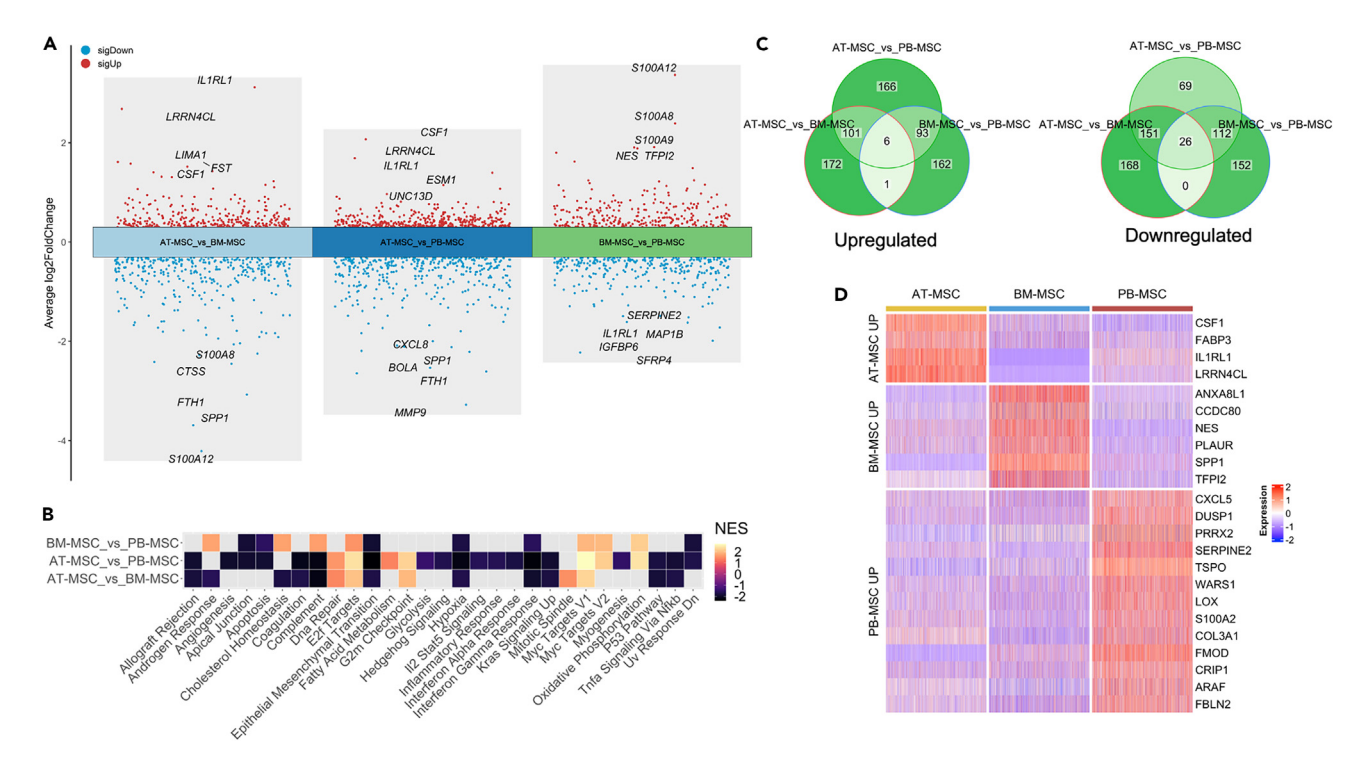


Figure 4. Bovine MSC express tissue-specific transcripts while also sharing enrichment for certain biological processes

(A) Volcano plot of pairwise differentially expressed gene (DEG) comparisons between AT-, BM-, and PB-MSC. Red dots indicate significantly upregulated genes whereas blue dots indicate those significantly downregulated. Y axis indicates log2 fold change.

(B) Gene Set Enrichment Analysis (GSEA) heatmap of biological processes across pairwise DEG comparisons. Normalized Enrichment Score (NES) is represented by the color key, indicating the enrichment score normalized to the number of genes in the set.

(C) Venn diagrams depicting the set sizes of upregulated and downregulated genes in each pairwise comparison of DEGs.

(D) Heatmap of the origin-tissue-specific upregulated DEGs among the three tissue sources. Relative expression is indicated by the color key. See also Figure S2 and Tables S1 and S2.

biological processes, gene set enrichment analysis was performed (Figure 4B). DNA repair, fatty acid metabolism, and G2M checkpoint were enriched in AT-MSC, while angiogenesis and apoptosis processes were associated with PB-MSCs. BM-MSCs showed specific enrichments for androgen response and cholesterol homeostasis.

Furthermore, the number of overlapping and unique DEGs across the pairwise comparisons was assessed (Figure 4C). Tissue origin-specific upregulated DEGs among MSC from the three tissues were identified (Figure 4D; Table S2). CSF1, FABP3, IL1RL1, and LRRN4CL showed a high expression in AT-MSCs specifically, whereas ANXA8L1, CCDC80, NES, PLAUR, SPP1, and TFPI2 were exclusively upregulated in BM-MSCs (Figure 4D). The highest number of tissue of origin-specific upregulated DEGs was observed in PB-MSCs, including CXCL5, DUSP1, PRRX2, SERPINE2, and FBLN2, among others (Figure 4D). Through gene ontology (GO) functional enrichment of the tissue of origin-specific upregulated DEGs, telomere maintenance and DNA biosynthetic processes were significantly enriched in AT-MSCs; whereas cell motility, vasculature development, and epithelial cell differentiation were significantly enriched in PB-MSCs (padj <0.05, Figure S2). BM-MSC-specific genes were related to immune response, cytoplasmic translation, and response to bacteria (padj <0.05, Figure S2).

To characterize the cellular interaction in bovine MSCs from different tissue origins, cell-cell communication analysis was performed using the CellChat package. An overview of the outgoing and incoming signaling patterns in AT-, BM-, and PB-MSCs was identified (Figures S3 and S4). Specifically, the main secreting signals of each of the annotated clusters were allocated into distinct signaling patterns (Figure 5A). In AT-MSC, MPZ, TENASCIN, and CDH signaling pathways were enriched in the CD29⁺⁺ MSC cluster, whereas the CD34⁺/CD105⁺ AT cluster secreted multiple signals, including LAMININ, FN1, THBS, SELE, and PECAM1 (Figure 5A). In BM-MSCs and PB-MSCs, LAMININ and VISFATIN were the common signals secreted by the CD29⁺⁺ MSC cluster and CXCL was secreted by the CD29⁺ MSC cluster (Figure 5A). Moreover, SPP1 and ADGRE5 pathways were detected in the macrophage/monocyte cluster of both BM- and PB-MSCs (Figure 5A). Furthermore, two common signaling pathways i.e., fibroblast growth factor (FGF) and fibronectin 1 (FN1), were selected and their contributions by cluster were assessed (Figure 5B). The CD29⁺⁺ and CD29⁺⁺ MSC clusters were the main source of FGF signals in MSCs from all three tissue sources, with a higher contribution of the CD29⁺⁺ MSC (Figure 5B). FGF is related to wound healing and angiogenesis, and FGF-2, in particular, is vital for maintaining MSC proliferation and differentiation potential. The FN1





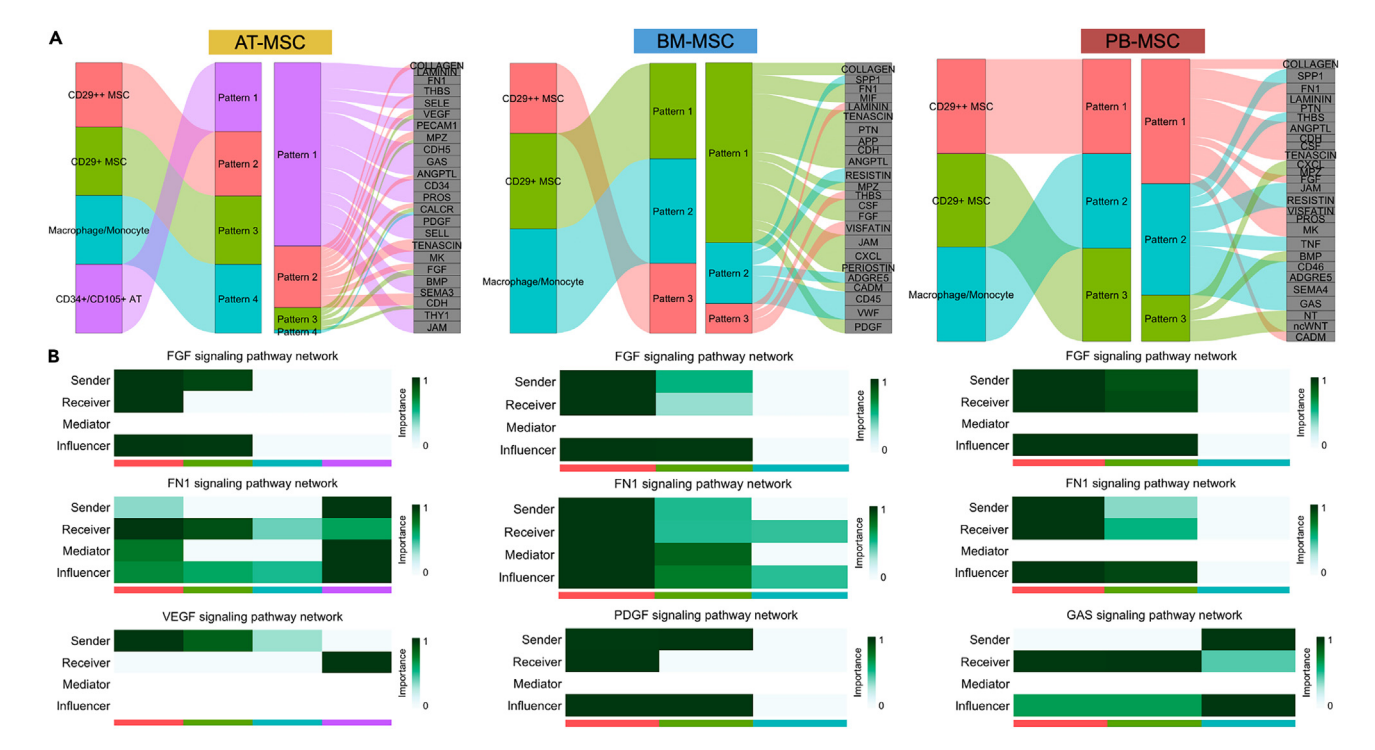


Figure 5. Cell-cell communication analysis of the main signaling pathways enriched in all three tissue sources

(A) River plots of each cluster were identified in each MSC tissue source correlating to their corresponding signaling pattern (left), followed by a river plot (right) of each signaling pattern and their relative composition of signaling pathways.

(B) In-depth analysis of two common signaling pathways across all three tissue sources (*FGF* and *FN1*), as well as one different pathway from each tissue source (*VEGF*, *PDGF*, and *GAS*). Color bars beneath each panel correspond to each MSC cluster (CD29++MSC: red; CD29+MSC: green; Macrophage/Monocyte: blue; CD34+/CD105+ AT: purple). See also Figures S3 and S4.

signaling pathway network was dominantly secreted by the CD29⁺⁺ MSC cluster in both BM- and PB-MSCs and by the CD34⁺/CD105⁺ AT cluster in AT-MSCs (Figure 5B).

In addition, one signaling pathway network that was unique to each tissue origin-specific MSCs was selected for further analysis. The vascular endothelial growth factor signaling pathway network was uniquely expressed in AT-MSCs, with the CD34⁺/CD105⁺ AT cluster as the major signal receiver (Figure 5B). This pathway has been reported to be critical to the differentiation of progenitor cells into endothelial cells. ⁴² In BM-MSCs, the platelet-derived growth factor (*PDGF*) signaling pathway was exclusively observed in the CD29⁺⁺ and CD29⁺⁺ MSC clusters, but absent in the macrophage/monocyte cluster, whereas the growth-arrest specific (*GAS*) signaling pathway network was specifically modulated by the macrophage/monocyte cluster in PB-MSCs (Figure 5B). The *PDGF* pathway is essential for growth and lineage differentiation in human BM-MSCs⁴³ and the *GAS* pathway has been shown to play a role in modulating inflammatory responses. ⁴⁴ Collectively, these results suggest that MSCs derived from different tissue sources possess both shared as well as unique signaling regulatory properties.

Exploring cellular lineage heterogeneity of tissue-specific MSCs

To explore the relation and lineage heterogeneity among cells in bovine MSCs, we performed pseudotime trajectory analysis of the three tissue-specific MSC populations using Monocle3⁴⁵ and the variable gene expression patterns were projected to UMAP for each tissue (Figure 6). To fully capture gene expression changes along the trajectory path, graph_test function was applied with the transcriptome data, and 4,993, 8,620, and 8,817 significantly DEGs (q_value <0.05) were identified in AT-MSCs, BM-MSCs, and PB-MSCs, respectively (Table S3). Through unsupervised hierarchical clustering analysis, these DEGs could be assigned to three modules within each tissue with similar expression pattern: one module exhibited high expression at the beginning, one module elevated expression at the middle point, while the remaining module showed extremely high expression at the end of the trajectory (Figure 6). Combined with functional enrichment analysis, we found the modules with similar expression pattern across the three tissues also shared common biological process. For instance, the module with the highest expression was related to positive regulation of epithelial to mesenchymal transition, and the module with the highest expression at later stages was involved with immune response (Table S3). Furthermore, the top 10 variable genes over trajectory for each tissue are highlighted in Figure S5. The results indicated that ferritin heavy chain 1 (*FTH1*) expression gradually increased along the trajectory path in BM-MSCs and PB-MSCs, while heat shock protein 47 (*SERPINH1*) expression decreased along the trajectory path in BM-MSCs.



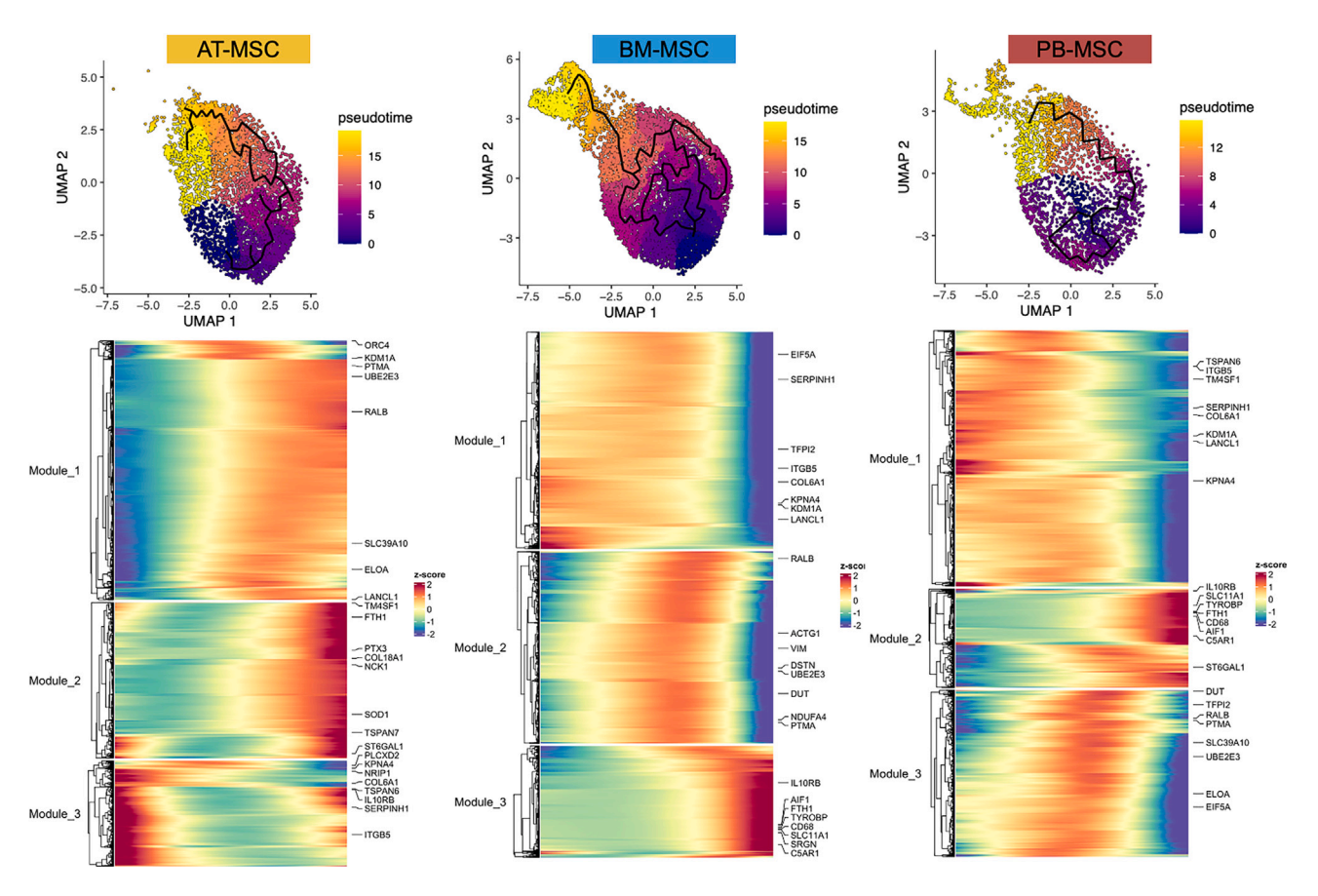


Figure 6. Trajectory analysis identifies cellular lineage heterogeneity and differentially expressed genes

Top: Tissue-specific UMAPs colored by trajectory. Bottom: Heatmap of the three identified modules of differentially expressed genes and their expression levels across trajectory for each tissue. See also Figure S5 and Table S3.

Species-specific gene expression patterns differentiate between bovine and equine donor-matched MSCs

Our group previously published an equine scRNA-seq dataset, from a single horse, comparing donor-matched MSCs from AT, BM, and PB that were isolated using the same protocols as used for the bovine donor-matched MSCs. ¹⁰ By converting the bovine gene names from the scRNA-seq dataset presented in this study to their equine orthologs, data from the bovine and equine datasets were plotted into one UMAP, and the differential expression of genes was compared both by species and by tissue source. Overall, approximately 20,000 bovine cells and 18,000 equine cells were plotted on a UMAP (Figure S6A), forming five distinct clusters with two clusters strongly overrepresented in one species and the other three clusters being mixed (Figures S6A, S6B, and S6C). No cluster was exclusively comprised of one tissue source (Figure S6D). UMAPs containing both bovine and equine MSCs and split by tissue origin type identified a more distinct localization of bovine MSCs when compared to equine MSCs (Figure 7A). Comparing gene overexpression in both species by tissue source revealed that all three bovine MSCs overexpressed *TMSB4X*, *NPAS2*, *ACTB*, and *GAPDH* relative to equine MSCs, whereas all three equine MSCs overexpressed *HSP90AB1* and transgelin (*TAGLN*) relative to bovine MSCs (Figure 7B). Additionally, certain tissue origin-specific genes such as *ATP5MC3*, *SPP1*, and *ARAF*, were enriched in bovine AT-MSCs, BM-MSCs, and PB-MSCs, respectively, and *B2M*, *SELENOW*, and *CTHRC1*, were enriched in equine AT-MSCs, BM-MSCs, respectively (Figure 7B).

Bovine BM-MSCs share more common features with human BM-MSCs when compared to murine BM-MSCs

Previously published scRNA-seq data from three human ⁴⁶ and ten murine ⁴⁷ donors of BM-MSCs were used for a comparative analysis with the bovine BM-MSC transcriptome obtained in this study. All gene names of the bovine and murine datasets were converted to their respective human orthologs for direct comparison. Approximately 40,000 human, 10,000 bovine, and 2,300 murine cells were analyzed (Figure S7A). Although clustering of individual cells was independent of species (Figures S7B and S7C), broad co-localization patterns by species were observed (Figures 8A and S7D). Moreover, a comparative pairwise DEG analysis between species showed that certain genes were enriched in a species-dependent manner (Figure 8B). Specifically, *NPAS2* was the most strongly enriched transcript in bovine BM-MSCs when compared to both human and mouse BM-MSCs, whereas *TAGLN* was more enriched in human BM-MSCs when compared to bovine and murine BM-MSCs (Figures 8B and 8C).





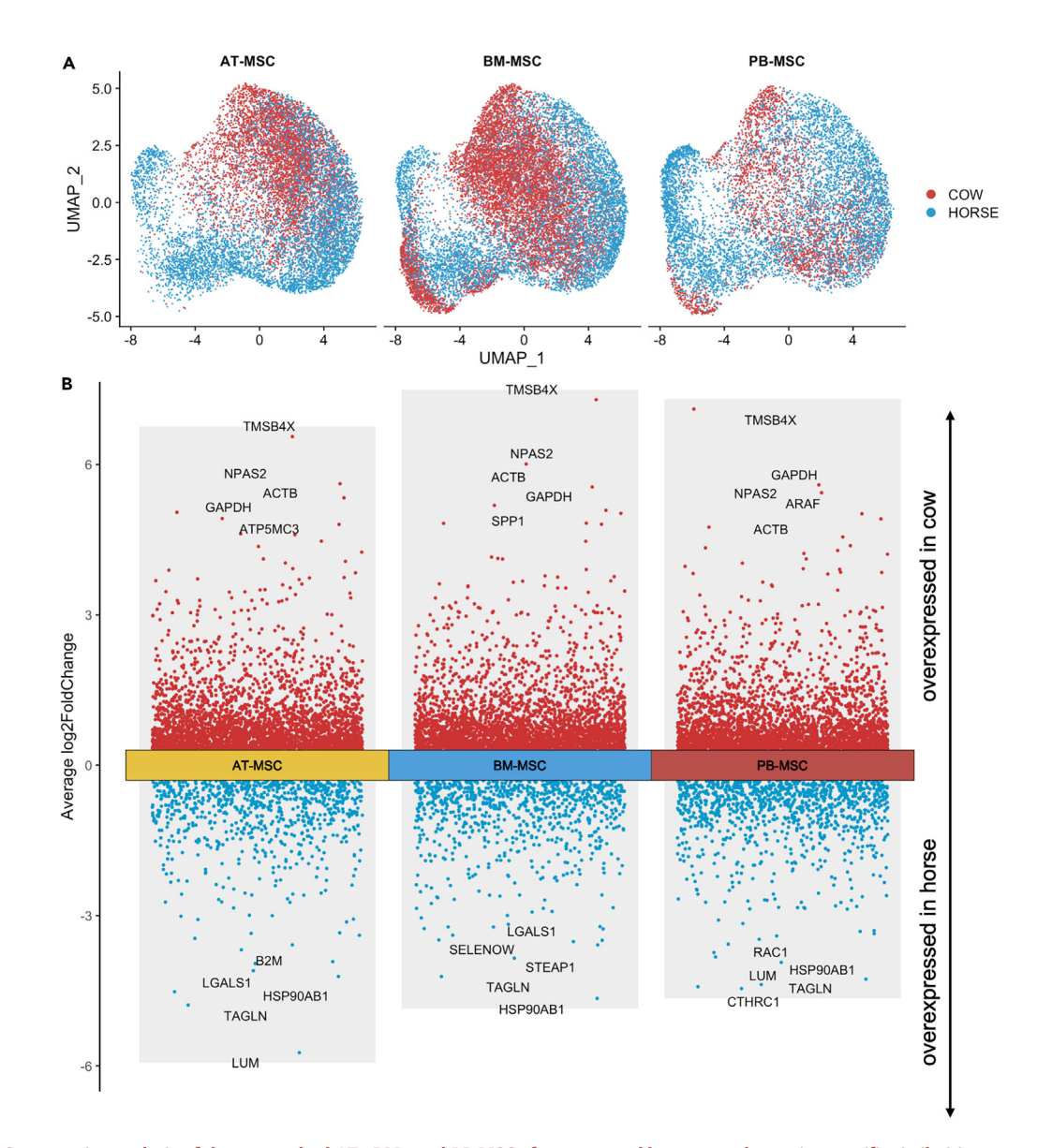


Figure 7. Comparative analysis of donor matched AT-, BM-, and PB-MSCs from cow and horse reveals species-specific similarities

(A) Heatmaps of each of the three tissue sources combine MSCs from both cows and horses. Red represents single cells from a cow and blue from a horse.

(B) Volcano plot indicating the genes overexpressed in cow or horse, split by tissue source. Red dots represent genes overexpressed in the cow; blue dots represent genes overexpressed in the horse. The y axis corresponds to log2 fold change in expression. See also Figure S6.

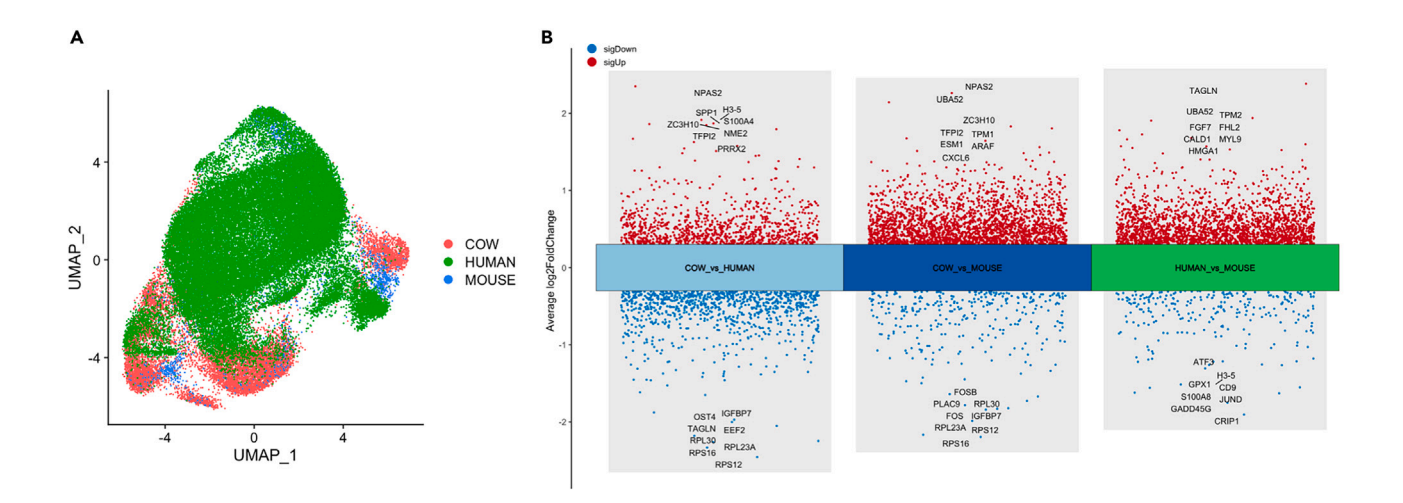
A further analysis of species-specific differences revealed 865 bovine-specific, 763 human-specific, and 165 murine-specific enriched transcripts in the combined BM-MSC dataset (Figure 8C; Table S4). An analysis of commonly expressed genes in BM-MSCs from the 3 species identified 297 genes, with most transcripts representing common housekeeping genes (C_1, Figure 8D). When comparing bovine and murine BM-MSCs, 70 transcripts were shared that also largely represented housekeeping genes (C_2, Figure 8D). Interestingly, the highest number of shared transcripts were found between bovine and human BM-MSCs, with 1,127 shared genes that were mostly related to MSC functions (C_3, Figure 8D). In contrast, murine and human BM-MSCs only shared 24 transcripts that were largely involved in housekeeping functions (C_4, Figure 8D). GO term enrichment identified common and unique enrichment of biological processes between the three species, including osteoblast differentiation in mice and cows, regulation of cytokinesis in humans and cows, and vasculature development in mice and humans (Figure S8).

DISCUSSION

In this work, bovine mesenchymal stromal cells (MSCs) were isolated from three different tissue sources—AT, BM, and PB—from one donor and subjected to scRNA-seq. In addition to evaluating both shared and tissue-specific transcriptomic patterns in the bovine MSCs, we used

iScience Article





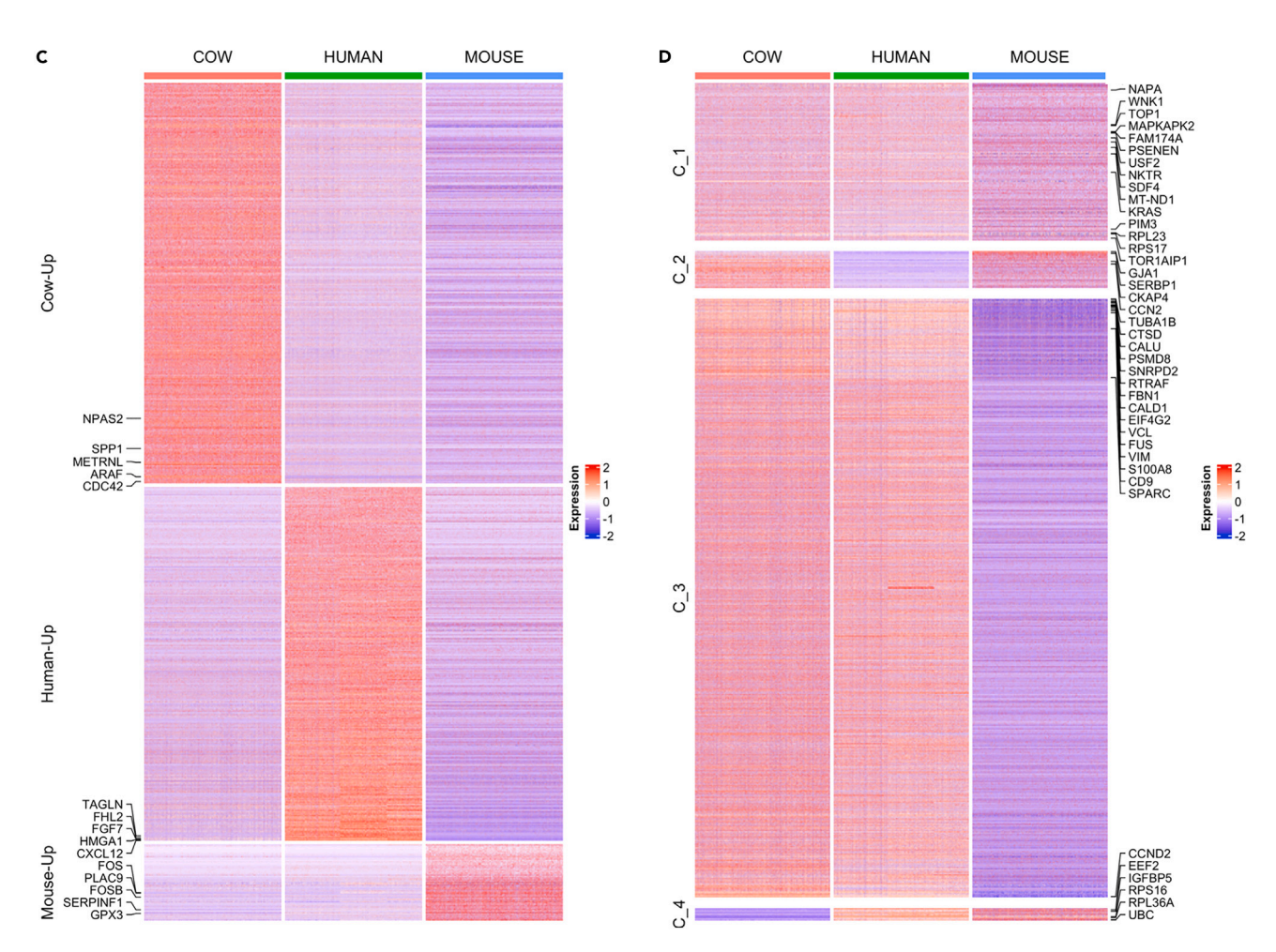


Figure 8. Comparative analysis of BM-MSCs from cow, human, and mouse reveals species-specific differences and shared features between the cow and human samples

(A) Heatmap of human, mouse, and cow BM-MSC samples combined, colored by species of origin.

(B) Volcano plot of pairwise differentially expressed genes between species. Red dots represent overexpressed genes; blue dots represent depleted genes. The y axis corresponds to log2 fold change in expression.





Figure 8. Continued

(C) Heatmap indicating the exclusively upregulated genes in each of the three species with highlights, with specific genes presented on the left.
(D) Heatmap indicating the shared genes between the different species. C_1 contains genes shared between all three species, C_2 corresponds to shared genes between the cow and mouse samples, C_3 indicates genes shared between the cow and human samples, and C_4 shows the gens shared between the human and mouse samples. Specific genes are highlighted on the right side. See also Figures S7 and S8 and Table S4.

this dataset to additionally perform transcriptomic comparisons with (i) equine AT-, BM-, and PB-MSCs, that we previously isolated using the same methodology and subjected to scRNA-seq¹⁰ and (ii) human and murine BM-MSCs using scRNA-seq datasets published by others. ^{46,47} A summary of all the cells and datasets used is included in Table 1. While using a single donor for the three bovine tissue sources is beneficial for inter-tissue comparisons, due to the elimination of donor-specific variations, further validation in multiple bovine donors may be required to make broader generalizations about the findings of this work.

We first combined the scRNA-seq from all bovine MSCs into one large dataset and found that MSCs from the three different tissue sources largely contained the same three clusters, namely a CD29⁺⁺ MSC, a CD29⁺⁺ MSC, and a macrophage/monocyte cluster. Macrophages/monocytes were identified in the dataset through the use of previously published marker sets in the equine and bovine models. ^{10,37,38} Consistent with bovine immunology studies, our macrophage/monocyte cluster expressed genes related to antigen presentation, such as *BOLA-DRA*, and CD68, a macrophage marker, was found to be more expressed overall in this cluster. ⁴⁸ Additionally, due to the relatively high expression of CD14 in this cluster, it can be inferred that the monocytes/macrophages that were isolated along with the MSC populations are of the classical monocyte type. ⁴⁹ An exception to the three major clusters was one unique small cluster, labeled CD34⁺/CD105⁺ AT, that was only expressed in AT-MSCs. This cluster was the only one to simultaneously express both the positive MSC markers CD105 and CD29, and the negative MSC marker CD34, as determined by the International Society for Cellular Therapy for human MSCs. ¹⁸ Interestingly, this marker expression profile is consistent with that of the stromal-vascular fraction (SVF), a type of heterogeneous cell population containing stem and progenitor cells, as well as endothelial and other cells, that can be isolated from adipose tissue. ⁵⁰ Indeed, a key hallmark of SVF, as well as early passage primary stromal cells that have been derived from adipose tissues, is the expression of CD34. ^{50,51} Additional studies showed that CD34 expression decreases with serial passaging of human adipose-derived stromal cells and typically persists up to 8–12 population doublings *in vitro*. ^{52,53}

When making pairwise comparisons between bovine MSCs from the different sources, we observed that fatty acid-binding protein 3 (*FABP3*) and interleukin 1 receptor-like 1 (*IL1RL1*) were significantly upregulated in AT-MSCs when compared to BM- and PB-MSCs. Specifically, *FABP3* can enhance both intracellular esterification and fatty acid uptake⁵⁴ and overexpression in human MSCs has been shown to inhibit their proliferation via negative regulation of cell cycle and downregulation of cell growth factors.⁵⁵ *IL1RL1* expression in AT-MSCs has been proposed to work with *IL-33* to regulate immune responses in the murine model.⁵⁶ In BM-MSCs, we found exclusively expressed secreted phosphoprotein 1, which is known to encode an extracellular matrix protein involved in regulating osteogenic differentiation of both human and porcine MSCs.^{57,58} Moreover, several genes of interest were overrepresented in bovine PB-MSCs compared to AT- or BM-MSCs as well. For example, C-X-C motif chemokine ligand 5 has been shown to mediate endogenous cell growth and migration.⁵⁹ Paired related homeobox 2 has DNA-binding transcription activity and its expression in MSCs was found to be associated with vasculogenesis during rat embryonic pituitary development.⁶⁰ Serine protease inhibitor clade E member 2 and fibulin-2 have been reported to promote osteoblast formation in human AT- and BM-MSCs, respectively.^{61,62}

Next, evaluating the intercellular signaling pathways in specific clusters showed that the dominant signaling pathways in the CD29⁺⁺ MSC cluster of AT-MSC were different from those of BM- or PB-MSCs. One example is the tenascin signaling pathway, which promotes cell adhesion and tissue remodeling, ⁶³ and tenascin-C has especially been reported to protect human BM-MSCs from death cytokines during *in vivo* implantation, ⁶⁴ to promote epithelial-to-mesenchymal transition, ⁶⁵ and to enhance the angiogenic and wound healing efficiency of both human BM- and equine PB-MSCs. ^{66,67} In contrast, the CD29⁺⁺ MSC cluster of bovine BM- and PB-MSCs shared secreting signaling networks, including the laminin and visfatin pathways. Laminin is an extracellular matrix protein that has been reported to promote the secretion of paracrine factors in human placenta-derived MSCs to repress cardiomyocyte apoptosis ⁶⁸ and visfatin regulates the cytokine and matrix-degrading enzyme profiles during osteogenic and adipogenic human MSC differentiation. ⁶⁹

In addition, by inferring the cellular lineage heterogeneity between different bovine MSC clusters, we identified distinct expression patterns along trajectory with associated genes showing dynamic expression. For example, *FTH1* showed the highest expression in the macrophage/monocyte cluster and is known to be related to macrophage activation, as well as protecting macrophages against iron-induced oxidative stress. On the other hand, serpin family H member 1 showed the lowest expression in the macrophage/monocyte cluster, but the highest expression in the CD29++ MSC cluster and is known to regulate collagen protein dynamics, including folding, secretion, and binding in the extracellular matrix, as well as promoting epithelial-to-mesenchymal transition.

Furthermore, the comparative analysis of scRNA-seq data from donor-matched bovine and equine MSCs from the three tissue sources, all cultured under the same conditions, revealed both similarities and differences across species. For example, thymosin beta 4 x-linked (TMSB4X) was strongly overexpressed in all three bovine MSCs when compared to their equine counterparts. TMSB4X encodes the thymosin $\beta4$ ($T\beta_4$) protein, a major actin-sequestering molecule in mammalian cells, 72 that has been shown to play a role in modulation of the inflammatory response, promotion of cell migration, angiogenesis, as well as stem cell regulation, and to enhance wound repair in animal clinical trials. $^{72-76}$ On the other hand, three equine MSCs overexpressed TAGLN, which also plays a role in actin binding. 77 Transgelin is associated with osteoblast and adipocyte differentiation in human stem cells and this protein has been proposed as a potential therapeutic to reduce elevated low-density lipoprotein cholesterol. 77,78 Future studies of bovine and equine MSCs could focus on the expression of these transcripts on the protein level and their stem cell-related functions, to explore their potential uses in veterinary and human medicine.





	Table 1. S	Summary	of all	species	donor	information,	MSC	culture	conditions,	and scRNA	A-seq dataset
--	------------	---------	--------	---------	-------	--------------	-----	---------	-------------	-----------	---------------

Species	Sex	Cell type	Number of individuals	Days in culture (passage)	Treatment	Number of cells analyzed	Sequencing depth (reads/cell)	Source
B. taurus	F	AT-MSC	1^	12 (p1)	None	6,121	31,264	This manuscript
		BM-MSC	1^	14 (p1)	None	10,497	18,965	This manuscript
		PB-MSC	1^	12 (p1)	None	3,076	57,270	This manuscript
E. caballus	F	AT-MSC	1*	19 (p3)	None	5,657	24,000	GSE156467
		BM-MSC	1*	19 (p3)	None	5,749	24,000	GSE156467
		PB-MSC	1*	19 (p1)	None	6,007	24,000	GSE156467
H. sapiens	N/R	BM-MSC	3	N/R (p1/p2)	None	41,401	59,675	GSE182158
M. musculus	М	BM-MSC	10	0 (p0)	None	2,614	160,000	GSE171530

^{^, * =} these samples are from the same animal (donor-matched).

Finally, using scRNA-seq datasets from bovine, human, and murine BM-MSCs further revealed species-specific differences. For example, the circadian clock gene neuronal PAS domain 2 (*NPAS2*), with a role in tumorigenesis and immune infiltration, ⁷⁹ was found to be overexpressed in bovine BM-MSCs when compared to both human and murine, as well as equine, BM-MSCs. *NPAS2* has been found to be upregulated in multiple cancers and to play a role in promoting cell survival by modulating the Warburg effect. ^{80,81} Future studies could focus on evaluating whether bovine BM-MSCs have a higher potential to support tumor formation ⁸² and/or if they co-opt cancer mechanisms to maintain their state of potency. One potential limitation of this work is that the bovine MSCs were cultured differently than the murine and human MSCs (Table 1), and MSCs were derived from individuals of different sex across species, which may influence the findings of the scRNA-seq. This could be mitigated in future studies by standardizing culture conditions and sex across species.

Our comparative analysis of BM-MSCs from different species demonstrated a greater similarity at the transcriptomic level between bovine and human BM-MSCs compared to murine and human BM-MSCs. This corroborates other studies reporting that bovine cells share more genomic and transcriptomic similarity with humans than the canonically used mouse model. ^{83–85} Moreover, the pool of shared genes between bovine and human BM-MSCs was composed of non-housekeeper genes, as opposed to the shared genes between humans and mice, but rather, it contained genes involved in reported properties and functions of MSCs, such as glutathione peroxidase 4, which is involved in maintaining a stemness phenotype, ⁸⁶ cellular communication network factor 2, which plays a significant role in MSC function in the BM, ⁸⁷ and fibrillin 1, which regulates stem cell differentiation, ⁸⁸ among others. Our findings further support the bovine model as a valuable translational animal model for MSC studies in human regenerative medicine.

Limitations of the study

This study used one biological donor for each analyzed MSC sample. Despite the benefits of donor-matching experimental design, ^{10,26,27} caution should be used when generalizing these findings without validation in MSCs from additional biological donors. Moreover, not all transcriptomic findings have been validated at the proteomic level, warranting confirmation in future studies.

STAR*METHODS

Detailed methods are provided in the online version of this paper and include the following:

- KEY RESOURCES TABLE
- RESOURCE AVAILABILITY
 - Lead contact
 - Materials availability
 - Data and code availability
- EXPERIMENTAL MODEL AND STUDY PARTICIPANT DETAILS
- METHOD DETAILS
 - O Isolation and culture of cells
 - Immunofluorescent staining
 - O Differentiation assays
 - O Single-cell RNA sequencing and analysis
 - Gene set enrichment analysis
 - O Pseudotime trajectory analysis using Monocle3

M = male, F = female.

AT = adipose tissue, BM = bone marrow, PB = peripheral blood.

N/R = not reported.





- O CellChat analysis
- O Comparative analysis across species
- O Quantitative PCR
- Flow cytometry
- QUANTIFICATION AND STATISTICAL ANALYSIS

SUPPLEMENTAL INFORMATION

Supplemental information can be found online at https://doi.org/10.1016/j.isci.2024.108886.

ACKNOWLEDGMENTS

The authors would like to thank Drs. Blake Nguyen, Daryl Nydam, Mason Jager, and Joy Tomlinson, as well as James Miller, for assisting with obtaining bovine tissue samples. We also thank Dr. Peter Schweitzer from the Cornell Institute of Biotechnology for preparing the single-cell library, conducting sequencing, and assisting with alignment.

This study was funded by the National Institute of Food and Agriculture, U.S. Department of Agriculture through a Hatch Grant # NYC-473426 to G.V.d.W., a grant from the Foundation for Food and Agricultural Research (FFAR) # CA20-SS-0000000004 to G.V.d.W., which includes matching funds from Elanco Animal Health Incorporated and New York Farm Viability Institute (NYFVI), and an NSF BII Grant (#2213824) to J.D.

AUTHOR CONTRIBUTIONS

Conceptualization, N.D. and G.V.d.W.; methodology, N.D., G.L., J.D., and G.V.d.W.; software, N.D. and G.L.; validation, N.D. and G.L.; formal analysis, N.D. and G.L.; investigation, N.D. and G.L.; resources, J.D. and G.V.d.W.; data curation, N.D. and G.L.; writing – original draft, N.D. and G.L.; writing – review & editing, N.D., G.L., J.D., and G.V.d.W.; visualization, N.D. and G.L.; supervision, J.D. and G.V.d.W.; project administration, J.D. and G.V.d.W.; funding acquisition, J.D. and G.V.d.W.

DECLARATION OF INTERESTS

The authors declare no competing interests.

Received: September 13, 2023 Revised: November 27, 2023 Accepted: January 8, 2024 Published: January 12, 2024

REFERENCES

- Harman, R.M., Marx, C., and Van de Walle, G.R. (2021). Translational Animal Models Provide Insight Into Mesenchymal Stromal Cell (MSC) Secretome Therapy. Front. Cell Dev. Biol. 9, 654885.
- Marx, C., Gardner, S., Harman, R.M., and Van de Walle, G.R. (2020). The mesenchymal stromal cell secretome impairs methicillinresistant Staphylococcus aureus biofilms via cysteine protease activity in the equine model. Stem Cells Transl. Med. 9, 746–757.
- 3. Harman, R.M., Churchill, K.A., Parmar, S., and Van de Walle, G.R. (2022). Mesenchymal stromal cells isolated from chicken peripheral blood secrete bioactive factors with antimicrobial and regenerative properties. Front. Vet. Sci. 9, 949836.
- Harman, R.M., Yang, S., He, M.K., and Van de Walle, G.R. (2017). Antimicrobial peptides secreted by equine mesenchymal stromal cells inhibit the growth of bacteria commonly found in skin wounds. Stem Cell Res. Ther. 8, 157.
- Bussche, L., Harman, R.M., Syracuse, B.A., Plante, E.L., Lu, Y.-C., Curtis, T.M., Ma, M., and Van de Walle, G.R. (2015).
 Microencapsulated equine mesenchymal stromal cells promote cutaneous wound healing in vitro. Stem Cell Res. Ther. 6, 66.

- Pang, S.H.M., D'Rozario, J., Mendonca, S., Bhuvan, T., Payne, N.L., Zheng, D., Hisana, A., Wallis, G., Barugahare, A., Powell, D., et al. (2021). Mesenchymal stromal cell apoptosis is required for their therapeutic function. Nat. Commun. 12, 6495.
- Galipeau, J., and Sensébé, L. (2018).
 Mesenchymal Stromal Cells: Clinical Challenges and Therapeutic Opportunities.
 Cell Stem Cell 22, 824–833.
- Lukomska, B., Stanaszek, L., Zuba-Surma, E., Legosz, P., Sarzynska, S., and Drela, K. (2019). Challenges and Controversies in Human Mesenchymal Stem Cell Therapy. Stem Cells Int. 2019, 9628536.
- Rizk, M., Monaghan, M., Shorr, R., Kekre, N., Bredeson, C.N., and Allan, D.S. (2016). Heterogeneity in Studies of Mesenchymal Stromal Cells to Treat or Prevent Graftversus-Host Disease: A Scoping Review of the Evidence. Biol. Blood Marrow Transplant. 22, 1416–1423.
- Harman, R.M., Patel, R.S., Fan, J.C., Park, J.E., Rosenberg, B.R., and Van de Walle, G.R. (2020). Single-cell RNA sequencing of equine mesenchymal stromal cells from primary donor-matched tissue sources reveals functional heterogeneity in immune modulation and cell motility. Stem Cell Res. Ther. 11, 524.

- Wright, A., Arthaud-Day, M.L., and Weiss, M.L. (2021). Therapeutic Use of Mesenchymal Stromal Cells: The Need for Inclusive Characterization Guidelines to Accommodate All Tissue Sources and Species. Front. Cell Dev. Biol. 9, 632717.
- Mushahary, D., Spittler, A., Kasper, C., Weber, V., and Charwat, V. (2018). Isolation, cultivation, and characterization of human mesenchymal stem cells. Cytometry A. 93, 19–31.
- da Silva Meirelles, L., Chagastelles, P.C., and Nardi, N.B. (2006). Mesenchymal stem cells reside in virtually all post-natal organs and tissues. J. Cell Sci. 119, 2204–2213.
- Shimoni, C., Goldstein, M., Ribarski-Chorev, I., Schauten, I., Nir, D., Strauss, C., and Schlesinger, S. (2020). Heat Shock Alters Mesenchymal Stem Cell Identity and Induces Premature Senescence. Front. Cell Dev. Biol. 8, 565970.
- Lange, C., Bassler, P., Lioznov, M.V., Bruns, H., Kluth, D., Zander, A.R., and Fiegel, H.C. (2005). Hepatocytic gene expression in cultured rat mesenchymal stem cells. Transplant. Proc. 37, 276–279.
- Martin, D.R., Cox, N.R., Hathcock, T.L., Niemeyer, G.P., and Baker, H.J. (2002). Isolation and characterization of multipotential mesenchymal stem cells from

iScience

Article



- feline bone marrow. Exp. Hematol. 30, 879–886.
- Klingemann, H., Matzilevich, D., and Marchand, J. (2008). Mesenchymal Stem Cells & ndash; Sources and Clinical Applications. Transfus. Med. Hemother. 35, 2.
- Dominici, M., Le Blanc, K., Mueller, I., Slaper-Cortenbach, I., Marini, F.C., Krause, D.S., Deans, R.J., Keating, A., Prockop, D.J., and Horwitz, E.M. (2006). Minimal criteria for defining multipotent mesenchymal stromal cells. The International Society for Cellular Therapy position statement. Cytotherapy 8, 315–317.
- Lin, C.-S., Ning, H., Lin, G., and Lue, T.F. (2012). Is CD34 truly a negative marker for mesenchymal stromal cells? Cytotherapy 14, 1159–1163.
- Heyman, E., Meeremans, M., Van Poucke, M., Peelman, L., Devriendt, B., and De Schauwer, C. (2023). Validation of multiparametric panels for bovine mesenchymal stromal cell phenotyping. Cytometry A. 103, 744–755.
- Mattar, P., and Bieback, K. (2015). Comparing the Immunomodulatory Properties of Bone Marrow, Adipose Tissue, and Birth-Associated Tissue Mesenchymal Stromal Cells. Front. Immunol. 6, 560.
- 22. Puissant, B., Barreau, C., Bourin, P., Clavel, C., Corre, J., Bousquet, C., Taureau, C., Cousin, B., Abbal, M., Laharrague, P., et al. (2005). Immunomodulatory effect of human adipose tissue-derived adult stem cells: comparison with bone marrow mesenchymal stem cells. Br. J. Haematol. 129, 118–129.
- 23. Ribeiro, A., Laranjeira, P., Mendes, S., Velada, I., Leite, C., Andrade, P., Santos, F., Henriques, A., Grãos, M., Cardoso, C.M.P., et al. (2013). Mesenchymal stem cells from umbilical cord matrix, adipose tissue and bone marrow exhibit different capability to suppress peripheral blood B, natural killer and T cells. Stem Cell Res. Ther. 4, 125.
- Xishan, Z., Baoxin, H., Xinna, Z., and Jun, R. (2013). Comparison of the effects of human adipose and bone marrow mesenchymal stem cells on T lymphocytes. Cell Biol. Int. 37, 11–18.
- Voga, M., Kovač, V., and Majdic, G. (2020). Comparison of Canine and Feline Adipose-Derived Mesenchymal Stem Cells/Medicinal Signaling Cells With Regard to Cell Surface Marker Expression, Viability, Proliferation, and Differentiation Potential. Front. Vet. Sci. 7, 610240.
- Mohamed-Ahmed, S., Yassin, M.A., Rashad, A., Espedal, H., Idris, S.B., Finne-Wistrand, A., Mustafa, K., Vindenes, H., and Fristad, I. (2021). Comparison of bone regenerative capacity of donor-matched human adiposederived and bone marrow mesenchymal stem cells. Cell Tissue Res. 383, 1061–1075.
- Alge, D.L., Zhou, D., Adams, L.L., Wyss, B.K., Shadday, M.D., Woods, E.J., Gabriel Chu, T.M., and Goebel, W.S. (2010). Donormatched comparison of dental pulp stem cells and bone marrow-derived mesenchymal stem cells in a rat model. J. Tissue Eng. Regen. Med. 4, 73–81.
- Pedersen, L.G., Castelruiz, Y., Jacobsen, S., and Aasted, B. (2002). Identification of monoclonal antibodies that cross-react with cytokines from different animal species. Vet. Immunol. Immunopathol. 88, 111–122.
- De Schauwer, C., Meyer, E., Van de Walle, G.R., and Van Soom, A. (2011). Markers of stemness in equine mesenchymal stem cells: a plea for uniformity. Theriogenology 75, 1431–1443.

- Chen, H., Ye, F., and Guo, G. (2019). Revolutionizing immunology with single-cell RNA sequencing. Cell. Mol. Immunol. 16, 242–249.
- 31. Food and Agricultural Organization, and Global Dairy Platform, Inc (2018). Climate Change and the Global Dairy Cattle Sector the Role of the Dairy Sector in a Low-Carbon Future.
- **32.** Interagency Agricultural Projections Committee (2021). USDA Agricultural Projections to 2030.
- 33. Cahuascanco, B., Bahamonde, J., Huaman, O., Jervis, M., Cortez, J., Palomino, J., Escobar, A., Retamal, P., Torres, C.G., and Peralta, O.A. (2019). Bovine fetal mesenchymal stem cells exert antiproliferative effect against mastitis causing pathogen Staphylococcus aureus. Vet. Res. 50, 25.
- 34. Mançanares, C.A.F., Oliveira, V.C., Oliveira, L.J., Carvalho, A.F., Sampaio, R.V., Mançanares, A.C.F., Souza, A.F., Perecin, F., Meirelles, F.V., Miglino, M.A., and Ambrósio, C.E. (2015). Isolation and characterization of mesenchymal stem cells from the yolk sacs of bovine embryos. Theriogenology 84, 887-898.
- 35. Khairoun, M., and S Korevaar, S. (2013). Human Bone Marrow- and Adipose Tissuederived Mesenchymal Stromal Cells are Immunosuppressive In vitro and in a Humanized Allograft Rejection Model. J. Stem Cell Res. Ther. 6, 20780.
- Hou, W., Duan, L., Huang, C., Li, X., Xu, X., Qin, P., Hong, N., Wang, D., and Jin, W. (2021). Cross-Tissue Characterization of Heterogeneities of Mesenchymal Stem Cells and Their Differentiation Potentials. Front. Cell Dev. Biol. 9, 781021.
- Danev, N., Harman, R.M., Oliveira, L., Huntimer, L., and Van de Walle, G.R. (2023). Bovine milk-derived cells express transcriptome markers of pluripotency and secrete bioactive factors with regenerative and antimicrobial activity. Sci. Rep. 13, 12600.
- Becker, D., Weikard, R., Hadlich, F., and Kühn, C. (2021). Single-cell RNA sequencing of freshly isolated bovine milk cells and cultured primary mammary epithelial cells. Sci. Data 8, 177.
- Finak, G., McDavid, A., Yajima, M., Deng, J., Gersuk, V., Shalek, A.K., Slichter, C.K., Miller, H.W., McElrath, M.J., Prlic, M., et al. (2015). MAST: a flexible statistical framework for assessing transcriptional changes and characterizing heterogeneity in single-cell RNA sequencing data. Genome Biol. 16, 278.
- 40. Jin, S., Guerrero-Juarez, C.F., Zhang, L., Chang, I., Ramos, R., Kuan, C.-H., Myung, P., Plikus, M.V., and Nie, Q. (2021). Inference and analysis of cell-cell communication using CellChat. Nat. Commun. 12, 1088.
- Yanada, S., Ochi, M., Kojima, K., Sharman, P., Yasunaga, Y., and Hiyama, E. (2006). Possibility of selection of chondrogenic progenitor cells by telomere length in FGF-2expanded mesenchymal stromal cells. Cell Prolif. 39, 575–584.
- Ge, Q., Zhang, H., Hou, J., Wan, L., Cheng, W., Wang, X., Dong, D., Chen, C., Xia, J., Guo, J., et al. (2018). VEGF secreted by mesenchymal stem cells mediates the differentiation of endothelial progenitor cells into endothelial cells via paracrine mechanisms. Mol. Med. Rep. 17, 1667–1675.
 Ng, F., Boucher, S., Koh, S., Sastry, K.S.R.,
- 43. Ng, F., Boucher, S., Koh, S., Sastry, K.S.R., Chase, L., Lakshmipathy, U., Choong, C., Yang, Z., Vemuri, M.C., Rao, M.S., and

- Tanavde, V. (2008). PDGF, TGF-β, and FGF signaling is important for differentiation and growth of mesenchymal stem cells (MSCs): transcriptional profiling can identify markers and signaling pathways important in differentiation of MSCs into adipogenic, chondrogenic, and osteogenic lineages. Blood 112, 295–307.
- 44. Decout, A., Katz, J.D., Venkatraman, S., and Ablasser, A. (2021). The cGAS–STING pathway as a therapeutic target in inflammatory diseases. Nat. Rev. Immunol. 21, 548–569.
- Trapnell, C., Cacchiarelli, D., Grimsby, J., Pokharel, P., Li, S., Morse, M., Lennon, N.J., Livak, K.J., Mikkelsen, T.S., and Rinn, J.L. (2014). The dynamics and regulators of cell fate decisions are revealed by pseudotemporal ordering of single cells. Nat. Biotechnol. 32, 381–386.
- Wang, Z., and Gong, G. (2023). Single-Cell Transcriptome Atlas of Human Mesenchymal Stem Cells (GSE182158) (Preprint).
- Kanazawa, S., Okada, H., Hojo, H., Ohba, S., Iwata, J., Komura, M., Hikita, A., and Hoshi, K. (2021). Mesenchymal stromal cells in the bone marrow niche consist of multi-populations with distinct transcriptional and epigenetic properties. Sci. Rep. 11, 15811
- properties. Sci. Rep. 11, 15811.

 48. Barut, G.T., Kreuzer, M., Bruggmann, R., Summerfield, A., and Talker, S.C. (2022). Single-cell transcriptomics reveals striking heterogeneity and functional organization of dendritic and monocytic cells in the bovine mesenteric lymph node. Front. Immunol. 13, 1099357.
- Talker, S.C., Barut, G.T., Lischer, H.E.L., Rufener, R., von Münchow, L., Bruggmann, R., and Summerfield, A. (2022). Monocyte biology conserved across species: Functional insights from cattle. Front. Immunol. 13, 889175.
- Bora, P., and Majumdar, A.S. (2017). Adipose tissue-derived stromal vascular fraction in regenerative medicine: a brief review on biology and translation. Stem Cell Res. Ther. 0.145
- 51. Bourin, P., Bunnell, B.A., Casteilla, L., Dominici, M., Katz, A.J., March, K.L., Redl, H., Rubin, J.P., Yoshimura, K., and Gimble, J.M. (2013). Stromal cells from the adipose tissue-derived stromal vascular fraction and culture expanded adipose tissue-derived stromal/stem cells: a joint statement of the International Federation for Adipose Therapeutics and Science (IFATS) and the International Society for Cellular Therapy (ISCT). Cytotherapy 15, 641–648.
- Maumus, M., Peyrafitte, J.-A., D'Angelo, R., Fournier-Wirth, C., Bouloumié, A., Casteilla, L., Sengenès, C., and Bourin, P. (2011). Native human adipose stromal cells: localization, morphology and phenotype. Int. J. Obes. 35, 1141–1153.
- Mitchell, J.B., McIntosh, K., Zvonic, S., Garrett, S., Floyd, Z.E., Kloster, A., Di Halvorsen, Y., Storms, R.W., Goh, B., Kilroy, G., et al. (2006). Immunophenotype of Human Adipose-Derived Cells: Temporal Changes in Stromal-Associated and Stem Cell-Associated Markers. Stem Cell. 24, 376–385.
- Matsumata, M., Inada, H., and Osumi, N. (2016). Fatty acid binding proteins and the nervous system: Their impact on mental conditions. Neurosci. Res. 102, 47–55.
- 55. Wang, S., Zhou, Y., Andreyev, O., Hoyt, R.F., Singh, A., Hunt, T., and Horvath, K.A. (2014). Overexpression of FABP3 inhibits human bone marrow derived mesenchymal stem cell



iScience Article

- proliferation but enhances their survival in hypoxia. Exp. Cell Res. 323, 56–65.
- 56. Liu, O., Xu, J., Wang, F., Jin, W., Zanvit, P., Wang, D., Goldberg, N., Cain, A., Guo, N., Han, Y., et al. (2021). Adipose-mesenchymal stromal cells suppress experimental Sjögren syndrome by IL-33-driven expansion of ST2+ regulatory T cells. iScience 24, 102446.
- 57. Mazzoni, E., Mazziotta, C., Iaquinta, M.R., Lanzillotti, C., Fortini, F., D'Agostino, A., Trevisiol, L., Nocini, R., Barbanti-Brodano, G., Mescola, A., et al. (2020). Enhanced Osteogenic Differentiation of Human Bone Marrow-Derived Mesenchymal Stem Cells by a Hybrid Hydroxylapatite/Collagen Scaffold. Front. Cell Dev. Biol. 8, 610570.
- Kannan, S., Ghosh, J., and Dhara, S.K. (2020). Osteogenic differentiation potential of porcine bone marrow mesenchymal stem cell subpopulations selected in different basal media. Biol. Open 9, bio053280.
- Kawata, K., Koga, H., Tsuji, K., Miyatake, K., Nakagawa, Y., Yokota, T., Sekiya, I., and Katagiri, H. (2021). Extracellular vesicles derived from mesenchymal stromal cells mediate endogenous cell growth and migration via the CXCL5 and CXCL6/CXCR2 axes and repair menisci. Stem Cell Res. Ther. 12, 414.
- 60. Higuchi, M., Kato, T., Yoshida, S., Ueharu, H., Nishimura, N., and Kato, Y. (2015). PRRX1and PRRX2-positive mesenchymal stem/ progenitor cells are involved in vasculogenesis during rat embryonic pituitary development. Cell Tissue Res. 361, 557–565.
- 61. Liu, J., He, S., Ma, B., Li, X., Wang, Y., and Xiong, J. (2023). TMT-based quantitative proteomic analysis revealed that FBLN2 and NPR3 are involved in the early osteogenic differentiation of mesenchymal stem cells (MSCs). Aging 15, 7637–7654.
- (MSCs). Aging 15, 7637–7654.

 62. Lin, K., Yang, Y., Cao, Y., Liang, J., Qian, J., Wang, X., and Han, Q. (2023). Combining single-cell transcriptomics and CellTagging to identify differentiation trajectories of human adipose-derived mesenchymal stem cells. Stem Cell Res. Ther. 14, 14.
- 63. Midwood, K.S., Chiquet, M., Tucker, R.P., and Orend, G. (2016). Tenascin-C at a glance.
 J. Cell Sci. 129, 4321–4327.
 64. Rodrigues, M., Yates, C.C., Nuschke, A.,
- 64. Rodrigues, M., Yates, C.C., Nuschke, A., Griffith, L., and Wells, A. (2013). The matrikine tenascin-C protects multipotential stromal cells/mesenchymal stem cells from death cytokines such as FasL. Tissue Eng. Part A 19, 1972–1983.
- Cheng, X., Li, F., and Tao, Z. (2021). Tenascin-C promotes epithelial-to-mesenchymal transition and the mTOR signaling pathway in nasopharyngeal carcinoma. Oncol. Lett. 22, 570.
- Sylakowski, K., Hwang, P., Justin, A., Shao, H., Whaley, D., Wang, Y., and Wells, A. (2022). Matricellular protein Tenascin-C enhances mesenchymal stem cell angiogenic and wound healing efficacy under ischemic conditions. J. Tissue Eng. Regen. Med. 16, 1249–1260.
- 67. Harman, R.M., HE, M.K., ZHANG, S., and VAN DE WALLE, G.R. (2018). Plasminogen activator inhibitor-1 and tenascin-C secreted by equine mesenchymal stromal cells stimulate dermal fibroblast migration in vitro and contribute to wound healing in vivo. Cytotherapy 20, 1061–1076.

- 68. Peng, K.-Y., Liu, Y.-H., Li, Y.-W., Yen, B.L., and Yen, M.-L. (2017). Extracellular matrix protein laminin enhances mesenchymal stem cell (MSC) paracrine function through ανβ3/CD61 integrin to reduce cardiomyocyte apoptosis. J. Cell Mol. Med. 21, 1572–1583.
- Tsiklauri, L., Werner, J., Kampschulte, M., Frommer, K.W., Berninger, L., Irrgang, M., Glenske, K., Hose, D., El Khassawna, T., Pons-Kühnemann, J., et al. (2018). Visfatin alters the cytokine and matrix-degrading enzyme profile during osteogenic and adipogenic MSC differentiation. Osteoarthritis Cartilage 26. 1225–1235.
- Mesquita, G., Silva, T., Gomes, A.C., Oliveira, P.F., Alves, M.G., Fernandes, R., Almeida, A.A., Moreira, A.C., and Gomes, M.S. (2020). H-Ferritin is essential for macrophages' capacity to store or detoxify exogenously added iron. Sci. Rep. 10, 3061.
- Tian, S., Peng, P., Li, J., Deng, H., Zhan, N., Zeng, Z., and Dong, W. (2020). SERPINH1 regulates EMT and gastric cancer metastasis via the Wnt/β-catenin signaling pathway. Aging 12, 3574–3593.
- Philp, D., and Kleinman, H.K. (2010). Animal studies with thymosin β4, a multifunctional tissue repair and regeneration peptide. Ann. N. Y. Acad. Sci. 1194, 81–86.
- N. Y. Acad. Sci. 1194, 81–86.
 Huff, T., Müller, C.S., Otto, A.M., Netzker, R., and Hannappel, E. (2001). β-Thymosins, small acidic peptides with multiple functions. Int. J. Biochem. Cell Biol. 33, 205–220.
- Goldstein, A.L., Hannappel, E., and Kleinman, H.K. (2005). Thymosin β: actin-sequestering protein moonlights to repair injured tissues. Trends Mol. Med. 11, 421–429.
- Crockford, D., Turjman, N., Allan, C., and Angel, J. (2010). Thymosin β4: structure, function, and biological properties supporting current and future clinical applications. Ann. N. Y. Acad. Sci. 1194, 179–189.
- Ehrlich, H.P., and Hazard, S.W., III (2010). Thymosin β4 enhances repair by organizing connective tissue and preventing the appearance of myofibroblasts. Ann. N. Y. Acad. Sci. 1194, 118–124.
- Lucero, D., Dikilitas, O., Mendelson, M.M., Aligabi, Z., Islam, P., Neufeld, E.B., Bansal, A.T., Freeman, L.A., Vaisman, B., Tang, J., et al. (2022). Transgelin: a new gene involved in LDL endocytosis identified by a genomewide CRISPR-Cas9 screen. J. Lipid Res. 63, 100160.
- 78. Elsafadi, M., Manikandan, M., Dawud, R.A., Alajez, N.M., Hamam, R., Alfayez, M., Kassem, M., Aldahmash, A., and Mahmood, A. (2016). Transgelin is a TGFB-inducible gene that regulates osteoblastic and adipogenic differentiation of human skeletal stem cells through actin cytoskeleston organization. Cell Death Dis. 7, e2321.
- Huang, Y., Xiao, L., Daba, M.Y., Xu, D., Wang, Y., Li, L., Li, Q., Liu, B., Qin, W., Zhang, H., and Yuan, X. (2023). Characterization of molecular subtypes based on chromatin regulators and identification of the role of NPAS2 in lung adenocarcinoma. Clin. Epigenetics 15, 72.
- 80. Ma, S., Chen, Y., Quan, P., Zhang, J., Han, S., Wang, G., Qi, R., Zhang, X., Wang, F., Yuan, J., et al. (2023). NPAS2 promotes aerobic glycolysis and tumor growth in prostate cancer through HIF-1A signaling. BMC Cancer 23, 280.

- 81. Yuan, P., Yang, T., Mu, J., Zhao, J., Yang, Y., Yan, Z., Hou, Y., Chen, C., Xing, J., Zhang, H., and Li, J. (2020). Circadian clock gene NPAS2 promotes reprogramming of glucose metabolism in hepatocellular carcinoma cells. Cancer Lett. 469, 498–509.
- Cuiffo, B.G., and Karnoub, A.E. (2012).
 Mesenchymal stem cells in tumor development. Cell Adh. Migr. 6, 220–230.
- 83. Jiang, Z., Sun, J., Dong, H., Luo, O., Zheng, X., Obergfell, C., Tang, Y., Bi, J., O'Neill, R., Ruan, Y., et al. (2014). Transcriptional profiles of bovine in vivo pre-implantation development. BMC Genom. 15, 756.
- 84. Everts-van der Wind, A., Larkin, D.M., Green, C.A., Elliott, J.S., Olmstead, C.A., Chiu, R., Schein, J.E., Marra, M.A., Womack, J.E., and Lewin, H.A. (2005). A high-resolution wholegenome cattle–human comparative map reveals details of mammalian chromosome evolution. Proc. Natl. Acad. Sci. USA 102, 18526–18531.
- 85. Bovine Genome Sequencing and Analysis Consortium, Elsik, C.G., Tellam, R.L., Worley, K.C., Gibbs, R.A., Muzny, D.M., Weinstock, G.M., Adelson, D.L., Eichler, E.E., Guigó, R., et al. (2009). The Genome Sequence of Taurine Cattle: A Window to Ruminant Biology and Evolution. Science 324, 522–528.
- 86. Peng, G., Tang, Z., Xiang, Y., and Chen, W. (2019). Glutathione peroxidase 4 maintains a stemness phenotype, oxidative homeostasis and regulates biological processes in Panc-1 cancer stem-like cells. Oncol. Rep. 41, 1264–1274.
- 87. Leguit, R.J., Raymakers, R.A.P., Hebeda, K.M., and Goldschmeding, R. (2021). CCN2 (Cellular Communication Network factor 2) in the bone marrow microenvironment, normal and malignant hematopoiesis. J. Cell Commun. Signal. 15, 25–56.
- 88. Smaldone, S., Clayton, N.P., del Solar, M., Pascual, G., Cheng, S.H., Wentworth, B.M., Schaffler, M.B., and Ramirez, F. (2016). Fibrillin-1 Regulates Skeletal Stem Cell Differentiation by Modulating TGFβ Activity Within the Marrow Niche. J. Bone Miner. Res. 31, 86–97.
- Hao, Y., Hao, S., Andersen-Nissen, E., Mauck, W.M., Zheng, S., Butler, A., Lee, M.J., Wilk, A.J., Darby, C., Zager, M., et al. (2021). Integrated analysis of multimodal single-cell data. Cell 184, 3573–3587.e29.
- Zappia, L., and Oshlack, A. (2018). Clustering trees: a visualization for evaluating clusterings at multiple resolutions. GigaScience 7, aiv083.
- Korotkevich, G., Sukhov, V., Budin, N., Shpak, B., Artyomov, M.N., and Sergushichev, A. (2021). Fast gene set enrichment analysis. Preprint at bioRxiv. https://doi.org/10.1101/ 060012.
- Liberzon, A., Birger, C., Thorvaldsdóttir, H., Ghandi, M., Mesirov, J.P., and Tamayo, P. (2015). The Molecular Signatures Database Hallmark Gene Set Collection. Cell Syst. 1, 417-425.
- Gu, Z., Eils, R., and Schlesner, M. (2016). Complex heatmaps reveal patterns and correlations in multidimensional genomic data. Bioinformatics 32, 2847–2849.
- 94. Yu, G., Wang, L.-G., Han, Y., and He, Q.-Y. (2012). clusterProfiler: an R Package for Comparing Biological Themes Among Gene Clusters. OMICS 16, 284–287.





STAR***METHODS**

KEY RESOURCES TABLE

REAGENT or RESOURCE	SOURCE	IDENTIFIER	
Antibodies			
Mouse Anti-CD73	Millipore	Cat# MABD122; RRID: AB_3083568	
Mouse Anti-CD44	BD	Cat# 550538; RRID: AB_393732	
Mouse Anti-CD29	Chemicon	Cat# CBL481; RRID: AB_93649	
Mouse Anti-CD90 conj. 488	Santa Cruz	Cat# SC-53116; RRID: AB_630310	
Mouse Anti-CD34	Thermo Fisher	Cat# MA1-10202; RRID: AB_11156010	
Mouse Anti-CD45	Santa Cruz	Cat# SC-18901; RRID: AB_627076	
Mouse Anti-CD79a conj. PE	Bio-Rad	Cat# MCA2538PE; RRID: AB_931716	
Goat Anti-mouse IgG (H+L) conj. 488	Jackson	Cat# 115-545-166; RRID: AB_2338852	
Mouse IgG1 isotype control	Abcam	Cat# ab18443; RRID: AB_2736846	
Chemicals, peptides, and recombinant proteins			
Heparin Sodium Salt	Sigma	Cat# H3149	
Phosphate Buffered Saline	Corning	Cat# 21-040-CM	
DMEM (low glucose)	Corning	Cat# 10-014-CV	
Fetal Bovine Serum	Atlanta Biologicals	Cat# S11150	
100X Penicillin/Streptomycin	GIBCO	Cat# 151400122	
100X Antibiotic/Antimycotic	Corning	Cat# 10-004-CI	
Glutamine	Corning	Cat# 25-005-CI	
Bovine Serum Albumin	Sigma	Cat# A4503-10G	
Ficoll-Paque Plus	GE Healthcare	Cat# 17-1440-02	
Collagenase Type 1	Worthington	Cat# CLS-1	
Dexamethasone	Sigma	Cat# D2915	
0.25% Trypsin, 0.1% EDTA in HBSS	Corning	Cat# 25-053-CI	
Adipogenesis Differentiation Medium	GIBCO	Cat# A10070-01	
Chondrogenesis Differentiation Medium	GIBCO	Cat# A10071-01	
Osteogenesis Differentiation Medium	GIBCO	Cat# A10072-01	
Alcian Blue 8GX	Sigma	Cat# A3157	
Dil Red O	Sigma	Cat# 00625	
Alizarin Red S	Sigma	Cat# A5533	
1% Paraformaldehyde	Thermo Scientific	Cat# J19943.K2	
Gill's Hematoxylin	Fisher	Cat# CS401-1D	
sopropanol	BDH Chemicals	Cat# 1174BDH	
Ethanol	Koptec	Cat# V1016	
Glacial acetic acid	J.T. Baker	Cat# 9526-03	
Glycerol mounting medium	DAKO	Cat# C0563	
SYTOX Orange Nucleic Acid Stain	Thermo Scientific	Cat# S11368	
Critical commercial assays			
Script cDNA Synthesis Kit	BIO-RAD	Cat# 1708891	
RNeasy Plus Micro Kit	Qiagen	Cat# 74034	
PowerTrack SYBR Green Master Mix	Applied Biosystems	Cat# A46109	
Chromium Next GEM Single Cell 3' GEM, Library & Gel Bead Kit v3.1	10x Genomics	Cat# 1000268	

(Continued on next page)





Continued			
REAGENT or RESOURCE	SOURCE	IDENTIFIER	
NextSeq 2K P3 100 bp kit	Illumina	Cat# 20046810	
Deposited data			
Single-cell RNA sequencing data from primary donor-matched bovine mesenchymal stromal cells (adipose, bone marrow and peripheral blood)	This manuscript	GEO: GSE241710	
Single-cell RNA sequencing data from primary donor-matched equine mesenchymal stromal cells (adipose, bone marrow and peripheral blood)	Harman et al., 2020	GEO: GSE156467	
Mesenchymal stromal cells in the bone marrow niche consist of multi-populations with distinct transcriptional and epigenetic properties [scRNA-Seq]	Kanazawa et al., 2021	GEO: GSE171530	
Single-Cell Transcriptome Atlas of Human Mesenchymal Stem Cells	Wang et al., 2021	GEO: GSE182158	
Experimental models: Cell lines			
Bovine Adipose Mesenchymal Stromal Cell	This manuscript	N/A	
Bovine Bone Marrow Mesenchymal Stromal Cell	This manuscript	N/A	
Bovine Peripheral Blood Mesenchymal Stromal Cell	This manuscript	N/A	
Experimental models: Organisms/strains			
Bos taurus, breed: Holstein-Frisian, sex: Female	N/A	NCBI: txid9913	
Equus caballus, breed: Warmblood, sex: Female	N/A	NCBI: txid9796	
Mus musculus, strain: C57BL/6JJcl, sex: Male	N/A	NCBI: txid10090	
Homo sapiens, sex: Unknown	N/A	NCBI: txid9606	
Oligonucleotides			
See Table S5 for qPCR oligonucleotides			
Software and algorithms			
Cellranger (v6.1.1)	10x Genomics	RRID:SCR_023221	
R Project for Statistical Computing (v4.2.2)	The R Foundation	RRID:SCR_001905	
RStudio (v2023.06.0+421)	Posit Software	RRID:SCR_000432	
Seurat (v4.3.0)	Satija Lab	RRID:SCR_016341	
clustree	Zappia and Oshlac	RRID:SCR_016293	
qqplot2	Posit Software	RRID:SCR_014601	
Monocle3 (v1.3.1)	Trapnell Lab	RRID:SCR_018685	
Biorender	Biorender	RRID:SCR_018361	
FACSDiva	BD	RRID:SCR_001456	
FlowJo (v10)		_	
	BD	RRID:SCR_008520 RRID:SCR_016137	
Excel (v16)	BD Microsoft	RRID:SCR_008520 RRID:SCR_016137	
Excel (v16) Prism (v10)	BD Microsoft GraphPad	RRID:SCR_008520 RRID:SCR_016137 RRID:SCR_002798	
Excel (v16) Prism (v10) MAST (1.24.1)	BD Microsoft GraphPad Bioconductor	RRID:SCR_008520 RRID:SCR_016137 RRID:SCR_002798 RRID:SCR_016340	
FlowJo (v10) Excel (v16) Prism (v10) MAST (1.24.1) ComplexHeatmap (v 2.14.0) scRNAtoolVis	BD Microsoft GraphPad Bioconductor Bioconductor	RRID:SCR_008520 RRID:SCR_016137 RRID:SCR_002798 RRID:SCR_016340 RRID:SCR_017270	
Excel (v16) Prism (v10) MAST (1.24.1) ComplexHeatmap (v 2.14.0) scRNAtoolVis	BD Microsoft GraphPad Bioconductor Bioconductor Zhang lab	RRID:SCR_008520 RRID:SCR_016137 RRID:SCR_002798 RRID:SCR_016340 RRID:SCR_017270 RRID:SCR_023916	
Excel (v16) Prism (v10) MAST (1.24.1) ComplexHeatmap (v 2.14.0) scRNAtoolVis fgsea (v 1.24.0)	BD Microsoft GraphPad Bioconductor Bioconductor Zhang lab Bioconductor	RRID:SCR_008520 RRID:SCR_016137 RRID:SCR_002798 RRID:SCR_016340 RRID:SCR_017270 RRID:SCR_023916 RRID:SCR_020938	
Excel (v16) Prism (v10) MAST (1.24.1) ComplexHeatmap (v 2.14.0) scRNAtoolVis	BD Microsoft GraphPad Bioconductor Bioconductor Zhang lab	RRID:SCR_008520 RRID:SCR_016137 RRID:SCR_002798 RRID:SCR_016340 RRID:SCR_017270 RRID:SCR_023916	

(Continued on next page)





Continued		
REAGENT or RESOURCE	SOURCE	IDENTIFIER
Other		
CKX41 Inverted Light Microscope	Olympus	RRID:SCR_023725
Fluoview FV300	Olympus	RRID: SCR_017015
Infinity2-1R USB Microscopy Camera	Lumenera	RRID:SCR_023724
Countess 3 FL Automated Cell Counter	Life Technologies	RRID:SCR_018591
5300 Fragment Analyzer System	Agilent Technologies	RRID:SCR_019411
NextSeq 2000 System	Illumina	RRID:SCR_023614
LSRFortessa Flow Cytometer	BD	RRID:SCR_019601
QuantStudio 3 Real Time PCR System	Life Technologies	RRID:SCR_018712
Cornell Institute of Biotechnology	Cornell University	RRID:SCR_021727

RESOURCE AVAILABILITY

Lead contact

Further information and requests for resources should be directed to and will be fulfilled by Dr. Gerlinde Van de Walle (grv23@cornell.edu).

Materials availability

Cell lines generated in this study will be shared by the lead contact upon request. No other unique regents were generated.

Data and code availability

- Single-cell RNA-seq data have been deposited at GEO under GSE241710 and are publicly available as of the date of publication. Accession numbers are listed in the key resources table. Flow cytometry and microscopy data reported in this paper will be shared by the lead contact upon request.
- This paper does not report original code.
- Any additional information required to reanalyze the data reported in this paper is available from the lead contact upon request.

EXPERIMENTAL MODEL AND STUDY PARTICIPANT DETAILS

A healthy, primiparous, lactating, female Holstein-Frisian cow (*Bos taurus*) was euthanized by captive bolt under Cornell University Institutional Animal Care and Use Committee (IACUC) protocol #2014-0038 by a licensed veterinarian. All experiments conducted were conformed to IACUC regulatory standards. Primary cells were derived from adipose tissue (AT) collected from the omental fat, bone marrow (BM) collected from the right femur, and peripheral blood (PB) collected from the coccygeal vein (the latter prior to euthanasia) and cultured in mesenchymal stromal cell (MSC) primary culture medium (consisting of DMEM (low glucose), supplemented with 30% Fetal Bovine Serum (FBS), 1X Penicillin/Streptomycin (P/S), 1X L-glutamine and 0.002% dexamethasone) until the first subculture, after which they were expanded in MSC expansion medium, consisting of MSC primary culture medium without dexamethasone. Growth conditions from isolation to expansion were maintained constant in an incubator at 37°C with 5% CO₂ saturation.

METHOD DETAILS

Isolation and culture of cells

Adipose tissue (AT)-MSCs were collected by harvesting approximately 10-15 g of AT from the omental fat and placed in a 50-mL conical tube with chilled 25 mL PBS and 2x Antibiotic/Antimycotic (AB/AM). Samples were transported on ice to sterile conditions and were minced using a sterile blade and scissors in a sterile petri dish over ice. Minced tissue was washed in PBS until parts separated. Upper phase contained AT and was used for downstream processing. AT was enzymatically digested in a solution of equal volume as the sample, containing 1% bovine serum albumin (BSA) and 0.1% collagenase type 1 in a 50-mL conical tube. Samples were agitated on a tube rotator at 37°C for at least 1 h (until sample was homogenized), after which tubes were filled to 45 mL with phosphate buffered saline (PBS). Each sample was centrifuged at 260 xg for 5 min at room temperature (RT), after which they were vortexed vigorously, and centrifuged again. After centrifugation, the supernatant was discarded, and the pellet was resuspended in 10 mL MSC primary culture medium, and cells were counted. Each resuspended pellet was plated in a T75 flask and incubated overnight at 37°C with 5% CO₂ saturation. After 24 h, medium was changed, and cells were monitored daily for colony formation. Upon the formation of 10 colonies per flask (approximately 8-12 days post-collection), cells were subcultured and replated in MSC expansion medium.

Bone marrow (BM)-MSCs were collected by aspirating 18 mL BM from the right femur in 60-mL syringes, pre-filled with 2 mL heparin diluted to 20,000 units/mL in PBS. Each 20 mL aspirate was transported on ice and dispensed into a T175 flask with 30 mL of MSC primary





culture medium. Flasks were left in an incubator at 37°C with 5% CO₂ saturation overnight. Next, 30 mL of pre-warmed MSC primary culture medium was added to each flask and the mixture was homogenized by pipetting. Then, 40 mL of homogenized mixture was aspirated from each flask and dispensed into a new flask. All flasks were incubated for 48 h, after which the supernatant was discarded, and flasks were washed with MSC primary culture medium to remove blood and other debris. After washing, medium was replaced with pre-warmed MSC primary culture medium and flasks were incubated for no more than 48 h at a time, after which the medium was changed again. Flasks were checked daily for the formation of colonies. Upon formation of more than 10 colonies in a flask (approximately 9-14 days post-collection), cells were passaged using trypsin, and re-plated in new T75 flasks in MSC expansion medium at a density of 5x10⁶ cells per flask. Cells were monitored daily with medium changes every 2-3 days and were subcultured upon reaching 80% confluence.

Whole blood was collected from the coccygeal vein in 15-mL vials with heparin to isolate peripheral blood (PB)-MSCs. Blood was transported on ice to sterile conditions and diluted 1:1 with PBS. Twenty mL of diluted blood was layered over 10 mL Ficoll-Paque Plus in 50-mL conical tubes and centrifuged at 1000 xg for 30 min at RT with the brake disabled. The buffy coat was removed and added to a new 50-mL conical flask containing 10 mL PBS. The flask was filled to 45 mL with PBS upon the addition of the buffy coat and centrifuged at 500 xg for 10 min at 4°C to remove platelets. The supernatant was discarded, pellets were resuspended in PBS, and cells were plated in T75 flasks at a concentration of 5x10⁷ cells per flask in MSC primary culture medium. Flasks were incubated overnight at 37°C with 5% CO₂ saturation. Cultures were checked daily for the appearance of colonies and medium was replenished every 48 h. Upon the formation of 10 colonies per flask (approximately 8-12 days post-collection), cells were subcultured in new flasks with MSC expansion medium.

Immunofluorescent staining

Confluent AT-, BM-, and PB-MSCs were washed with PBS, detached with trypsin, and centrifuged at 300 xg for 5 min at RT. Approximately 15,000 MSCs were plated in wells of a 4-well plate fitted with 13 mm² sterile glass coverslips. Each well was used for a different antibody – CD73, CD44, CD29 and isotype, with three total plates used – one for each tissue source. Two days after plating, cells were pre-fixed in 2% paraformaldehyde (PFA) in MSC medium for 5 min, followed by a 5-min fixing step in 4% PFA in PBS. Cells were then permeabilized in 0.2% Triton-X in PBS for 10 min and washed twice in PBS for 5 min. PBS with 10% BSA was used as a blocking buffer for 30 min at RT. Antibodies were diluted at 1:250 in PBS and cells were incubated with primary antibody solution overnight at 4°C. Cells were then washed 3 times with PBS, for 5 min each time, and then incubated with secondary antibody, diluted 1:500 in PBS, for 1 h at RT. Cells were washed 3 times in PBS, for 5 min each time, and then incubated in 1:30,000 SYTOX Orange in PBS for 6 min. Finally, cells were washed 3 times in deionized water, for 5 min each, and coverslips were mounted on to glass slides using aqueous mounting medium. After drying overnight, imaging was performed on an Olympus confocal microscope, and post-imaging processing was completed in FIJI.

Differentiation assays

Confluent AT-, BM-, and PB-MSCs were washed with PBS, detached with trypsin, and centrifuged at 300 xg for 5 min at RT. MSCs were plated in wells of a 24-well plate fitted with 13 mm² sterile glass coverslips.

For differentiation into adipocytes, 15,000 MSCs were seeded over the entire surface of a coverslip and allowed to adhere in MSC expansion medium for 2 h in an incubator. For differentiation into chondrocytes, 5 droplets of 5 µL MSC expansion medium containing 15,000 cells each were seeded on a coverslip and allowed to adhere for 2 h. For differentiation into osteocytes, 10,000 cells were seeded over the entire surface of a coverslip and allowed to adhere in MSC expansion medium. Each MSC culture was plated in triplicate for differentiation, and also in triplicate for control imaging. Upon adhesion to the coverslip, MSC expansion media was aspirated and replaced with either Adipogenesis, Chondrogenesis, or Osteogenesis media. Controls were grown in MSC expansion media. Adipocytes and chondrocytes were left to differentiate for 8 and osteocytes for 14 days, respectively, with media replacement every 3-4 days. Coverslips were rinsed with PBS, fixed using 4% paraformaldehyde (PFA) by incubating for 10 min at RT, washed 3x with PBS for 5 min each, and stored in sterile water at 4°C until staining. For adipocyte staining, 3 mL Oil Red O was diluted in 2 mL sterile water and filtered to generate a working solution. Water was aspirated from coverslips and replaced with 60% isopropanol and incubated for 5 min. Isopropanol was removed and replaced with Oil Red O working solution and incubated for 15 min at RT. Upon incubation, coverslips were washed with sterile water twice for 5 min and incubated overnight at RT in Alcian Blue and then washed twice in destaining solution (60% ethanol/40% glacial acetic acid) for 20 min. Coverslips were washed with sterile water twice. For osteocyte staining, coverslips were incubated in Alizarin Red for 45 min in the dark at RT and then washed with sterile water four times for 5 min each.

Upon completion of staining, each sample was mounted on a slide using DAKO Glycerol Mounting medium and imaged on a light microscope.

Single-cell RNA sequencing and analysis

Upon 80% confluence of first subcultures of bovine AT-, BM-, and PB-MSCs, cells were trypsinized and diluted in PBS to a final concentration of 8x10⁵ cells/mL. Cell viability was confirmed to be greater than 80% using an Invitrogen Countess 3 FL automated cell counter and a library was generated using the 10x Genomics Chromium Next GEM Single-cell 3' v3.1 assay, following manufacturer instructions. Upon creation of the cDNA library, a quality control step was performed using an Agilent Technologies Fragment Analyzer System to verify quality and concentration. Sequencing was performed on an Illumina NextSeq 2000 sequencer using the Illumina NextSeq 2K P3 100 bp kit following recommendations by 10x Genomics protocols.





We performed sequence alignment to the bovine reference genome (ARS-UCD 1.2, Ensembl database) using the CellRanger (v 6.1.1) software from 10X Genomics with the protein_coding attribute. The output feature-barcode matrices were read into R (v 4.2.2), excluding any cell expressing fewer than 200 genes and any gene expressed in fewer than 3 cells (per tissue source). Next, quality control and visualization were performed using Seurat (v 4.3.0). Cells with fewer than 1,000 or more than 40,000 nCount_RNA were filtered out, and cells with more than 6,000 features were also removed. Similarly, cells with greater than 15% mitochondrial mapping were filtered out, leading to 6121, 10497 and 3076 cells in AT-, BM-, and PB-MSCs, respectively. The sequencing batch, cell cycle score, nFeature_RNA, percent of mitochondrial and ribosomal genes were considered during normalization process, and the integration of the three datasets was conducted using the IntegrateData function with 5,000 variable features. For identifying cell clusters, the optimal resolution was calculated by clustree package and the dimensionality reduction was performed with the top 25 principal components. To annotate the cell clusters, the FindAllMarkers function with default parameters was used to help defining cluster identity. Each cluster was named using canonical markers used to identify veterinary and human cells. 10,18,37,51

Gene set enrichment analysis

GSEA was performed using fgsea package (v 1.24.0)⁹¹ with the hallmark gene set data from MSigDB.⁹² For each comparison, genes were ordered by log2(FC) of model-based analysis of single-cell transcriptomics (MAST) results and the analysis was performed with 1000 permutations. Conversions between bovine and human annotation was performed using biomaRt (v 2.54.1).

Pseudotime trajectory analysis using Monocle3

To infer the cellular lineage heterogeneity for each tissue, we followed the standard workflow of Monocle3 (v 1.3.1)⁴⁵ to conduct pseudotime trajectory analysis. We selected the CD29⁺⁺ MSC cluster as the start point of pseudotime and the trajectory path calculated by Monocle3 agreed with the cluster identities. Spatial differential expression analysis along the trajectory was performed with graph_test function in Monocle3 and trajectory-dependent genes were obtained (q value <0.05). For each tissue, the set of genes was divided into three modules along the trajectory using unsupervised hierarchical clustering and visualized by ComplexHeatmap (v 2.14.0).⁹³

CellChat analysis

The mouse ligand-receptor interaction database was used in this study, and conversion between murine and human annotation was performed using biomaRt (v 2.54.1). We followed the CellChat (v1.6.1)⁴⁰ tutorial to obtain the cellular signaling pathways across different cell types and also performed comparison among tissue sources. Briefly, the CellChat object was created from Seurat object for each tissue, and then all CellChat objects were merged together for comparative analysis. We inferred the cellular communication network across the four cell types and the communication probability was calculated using computeCommunProb function. The network centrality scores for target signaling pathway were calculated to check the contributions of each cell type. The dominant secreting signals of each cell type was obtained using identifyCommunicationPatterns function.

Comparative analysis across species

The equine AT-, BM-, and PB-MSC datasets were obtained from the NCBI GEO database. ¹⁰ The BM-MSC datasets from human ⁴⁶ and mouse ⁴⁷ were also downloaded from NCBI GEO. Firstly, the one-to-one ortholog gene list across the four species was obtained using biomaRt (v 2.54.1). Secondly, the low-quality cells and the gene-cell expression matrices were filtered and obtained by aligning the sequencing data to the corresponding reference genome. Thirdly, the gene-cell expression output was modified by only keeping the one-to-one ortholog genes across species. Fourthly, the modified gene-cell expression matrices were used as inputs to create a Seurat object for each species. Finally, multiple Seurat objects were merged using the same methods as above, and differential expression analysis was performed by MAST to get the species-specific and commonly expressed genes.

Quantitative PCR

Upon 80% confluence, cells were detached using trypsin and washed with PBS by centrifugation at room temperature for 5 minutes at 300 xg. RNA was extracted from each centrifuged pellet using the Qiagen RNeasy Mini Plus kit, following manufacturer's instructions. Upon isolation, RNA was quantified on a Thermo Fisher NanoDrop Spectrophotometer and converted to cDNA using the Biorad iScript gDNA Clear cDNA synthesis kit, following the manufacturer's instructions. Primers were at a final concentration of 0.3 μ M and Applied Biosystems PowerTrack SYBR Green MasterMix was used in a 96-well plate. The reaction was performed in an Applied Biosystems QuantStudio 3 thermal cycler. Data was analyzed using Microsoft Excel and visualized in GraphPad Prism. Primer sequences and sources are listed in Table S5.

Flow cytometry

Bovine AT-, BM-, and PB-MSCs were cultured in T75 flasks until 80% confluence and then detached using trypsin. Pellets were resuspended in PBS supplemented with 1% BSA (PBS/BSA), counted, and approximately 100,000 cells per sample were dispensed into 4-mL flow cytometry tubes. Each sample was centrifuged at 300 xg for 7 min at 4° C and then resuspended in 50 μ L of the appropriate primary antibody, diluted in PBS/BSA. Cells with primary antibodies were incubated for 1 h on ice, after which each sample was filled with 2 mL ice cold PBS/BSA and centrifuged at 300 xg for 7 min at 4° C. Supernatants were discarded and pellets resuspended in 50 μ L secondary antibody (diluted in





PBS/BSA). Cells were incubated for 20 min on ice, washed with 2 mL ice cold PBS/BSA, resuspended in $400 \, \mu L$ PBS/BSA, and analyzed on a BD LSRFortessa flow cytometer. BD FACSDiva software was used to operate the flow cytometer. After data collection, downstream analysis was performed on BD FlowJo software. Final visualization was done in GraphPad Prism.

QUANTIFICATION AND STATISTICAL ANALYSIS

Differential expression was performed using MAST (1.24.1), 39 with random effect for sequencing depth. Genes were considered significant if the adjusted P value was < 0.05 and the log2(fold change) was > 0.3 or < -0.3. The visualization of DEGs was performed with the scRNAtoolVis package. The functional enrichment analysis of selected gene lists was performed using clusterProfiler package (v 4.6.2). 94 The visualization of gene expression patterns across tissue types or species was done by ComplexHeatmap (v 2.14.0). 93